Global study of a family of cubic Liénard equations

Alexander Khibnik* Bernd Krauskopf† Christiane Rousseau‡§

CRM-2471
April 1997

*Theory Center, Cornell University, Ithaca, NY 14853, U.S.A., khibnik@cam.cornell.edu
†Physics and Astronomy, Vrije Universiteit, 1081 HV Amsterdam, The Netherlands, berndk@nat.vu.nl
‡Dép. de Math. & Stat. et CRM, Université de Montréal, Montréal, QC H3C 3J7, Canada, rousseac@ere.umontreal.ca
§This work was supported by NSERC and FCAR in Canada.

Abstract

We derive the global bifurcation diagram of a three-parameter family of cubic Liénard systems. This family seems to have a universal character in that its bifurcation diagram (or parts of it) appears in many models from applications. In fact, it is the 3-jet of a three-dimensional slice of the universal unfolding of a doubly degenerate Bogdanov-Takens point, that is, of the codimension-four singularity with nilpotent linear part and no quadratic terms in the normal form.

AMS classification. 58F14, 58F21, 34C20, 58F40

Résumé

On trouve le diagramme de bifurcation d'une famille à trois paramètres de systèmes de Liénard cubiques. Le diagramme de bifurcation de cette famille (ou des morceaux importants de ce diagramme) semble avoir un caractère universel, en ce sens qu'il apparait dans de nombreux modèles venant des applications. En fait c'est le 3-jet d'une sous-famille à trois paramètres du déploiement universel d'une singularité nilpotente de codimension 4, pour laquelle les deux termes quadratiques de la forme normale sont nulles.

1 Introduction

There are some two-dimensional bifurcation diagrams of planar vector fields that seem to have a "universal character" in the sense that they occur in many models from applications. In this paper we consider such an example, namely the bifurcation diagram sketched in Figure 1 which has been observed in models of electrical circuits [Ba75], as well as chemical [KBY87, VSA78, BDK80], biochemical [KS75] and ecological models [BBIK93]. In all these examples one may find three different singular points, one saddle and two antisaddles. There is a possibility of one or two large limit cycles surrounding the three singular points. If there is one large limit cycle then there can also exist two small limit cycles, one around around each antisaddle. If there are two large limit cycles then there can also exist one small limit cycle surrounding one antisaddle.

What is the mathematical reason for the observed universality? It appears natural to expect that the examples mentioned above arise in the unfolding of some local or global singularity. The singularities of planar vector fields of codimension less than or equal to three can only be of three types: semi-hyperbolic points, weak foci, or nilpotent points; see for example [AAIS94, Ku95]. In the latter case there are four types of codimension-three singularities: the cusp of order three [DRS87, BK85, BKK85], and the focus, saddle and elliptic nilpotent points [DRS91, BKK85]. (Recall that a cusp of order three is the singularity one gets when the xy-term vanishes in the Bogdanov-Takens normal form $\dot{x} = y,\ \dot{y} = ax^2 + bxy$. For the other three singularities the x^2-term in this normal form vanishes, and they constitute the different cases in terms of the corresponding 3-jet.) None of the unfoldings of these singularities has the dynamical richness of the examples we are considering. Consequently, we expect a singularity of codimension at least four to lurk in the background as an organizing center.

As part of the examples one finds the unfolding of a codimension-two nilpotent singularity in the class of $\mathbf{Z}_2$-equivariant planar vector field, where the symmetry is the rotation by π; see [Ca81, Kh85]. This singularity has a 3-jet which is C^∞-equivalent to

$$\begin{aligned} \dot{x} &= y \\ \dot{y} &= -x^3 - x^2 y. \end{aligned} \tag{1.1}$$

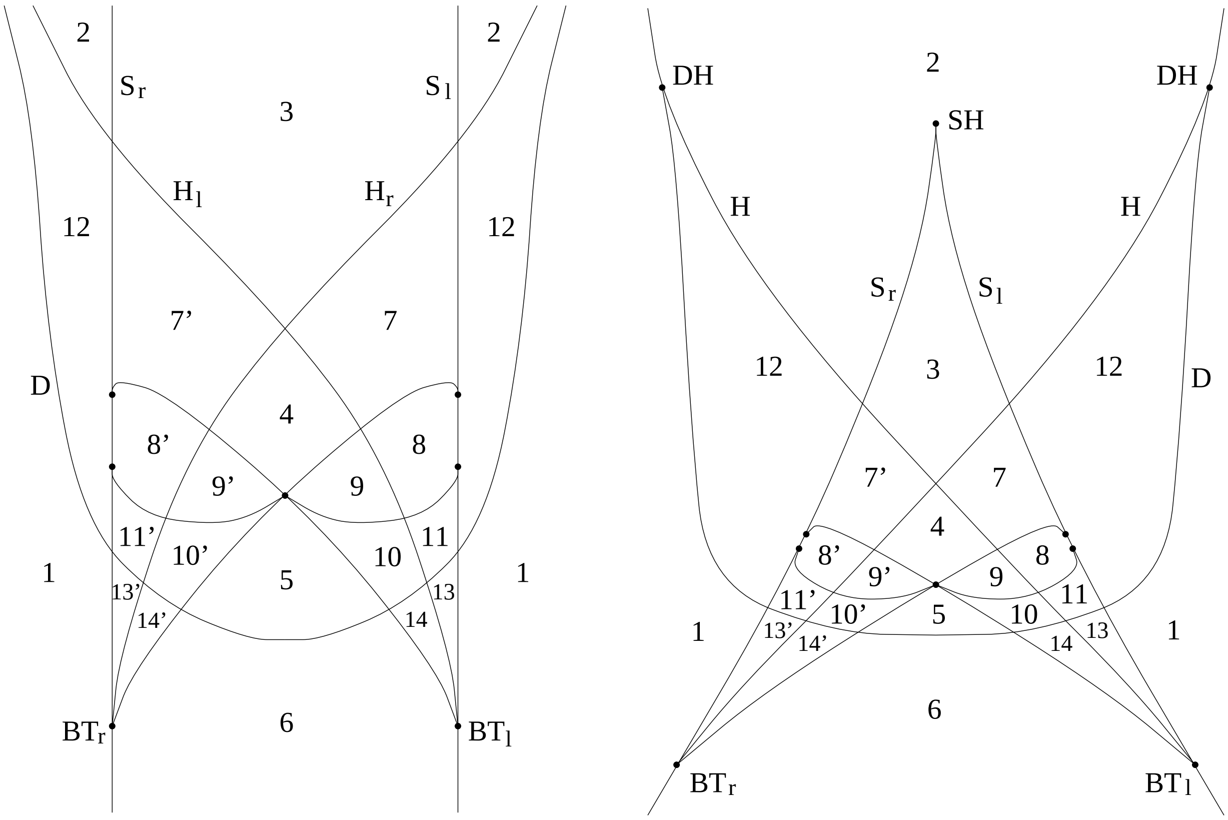

Figure 1: Bifurcation diagrams that are topologically like these two can be found in the literature for many different applications. (For the corresponding phase portraits see Figure 2.) The two diagrams are sketches of sections through the bifurcation diagram of (1.2) for $\mu_2 = const > 0$ (left) and for $\mu_3 = const > 0$ (right).

This suggests to consider the singularity with 3-jet given by (1.1), which is of codimension four in the class of all planar vector fields. Note that (1.1) is the 3-jet of a doubly degenerate Bogdanov-Takens point with no quadratic terms in the normal form.

In this paper we consider the global three-parameter partial unfolding of (1.1) given by the family

$$\begin{aligned} \dot{x} &= y \\ \dot{y} &= \mu_1 + \mu_2 x + \mu_3 y - x^3 - x^2 y, \end{aligned} \tag{1.2}$$

for which we have the following.

Result:
The global bifurcation diagram of (1.2) has conic structure and its intersection with any sphere around the central singularity (1.1) is topologically like shown in Figure 2 as a projection of the sphere minus a point onto the plane. We conjecture that the bifurcation diagram of (1.2) in Figure 2 is complete.

This result falls short of a theorem. Numerical methods yield the exact positions of the curve D of double limit cycles and the different curves of homoclinic loops. The conjectural part is concerned with the curve of double limit cycles. It is conjectured that there is a unique connected curve of double limit cycles going from one degenerate Hopf bifurcation to the other. The part of the connected curve inside the region with three singular points is known as well as its respective position with respect to all homoclinic loops. However, this is still an open question in the region with one singular point. In some regions the number of limit cycles is precisely known, but their hyperbolicity is not proved in all cases.

A quantitative picture of the bifurcation diagram is shown in Figure 3 as a projection onto the plane. An interactive 3D-viewer and a movie of the bifurcation set in (μ_1, μ_2, μ_3)-space can be found at
`http:www.nat.vu.nl/~berndk/kkr/kkr.html`.

In fact (1.2) (and not the full codimension-four unfolding) represents the simplest mathematical model that contains the dynamical richness of the examples above. In particular, for $\mu_1 = 0$ we find the $\mathbf{Z}_2$-equivariant unfolding of (1.1), which is shown in Figure 4.

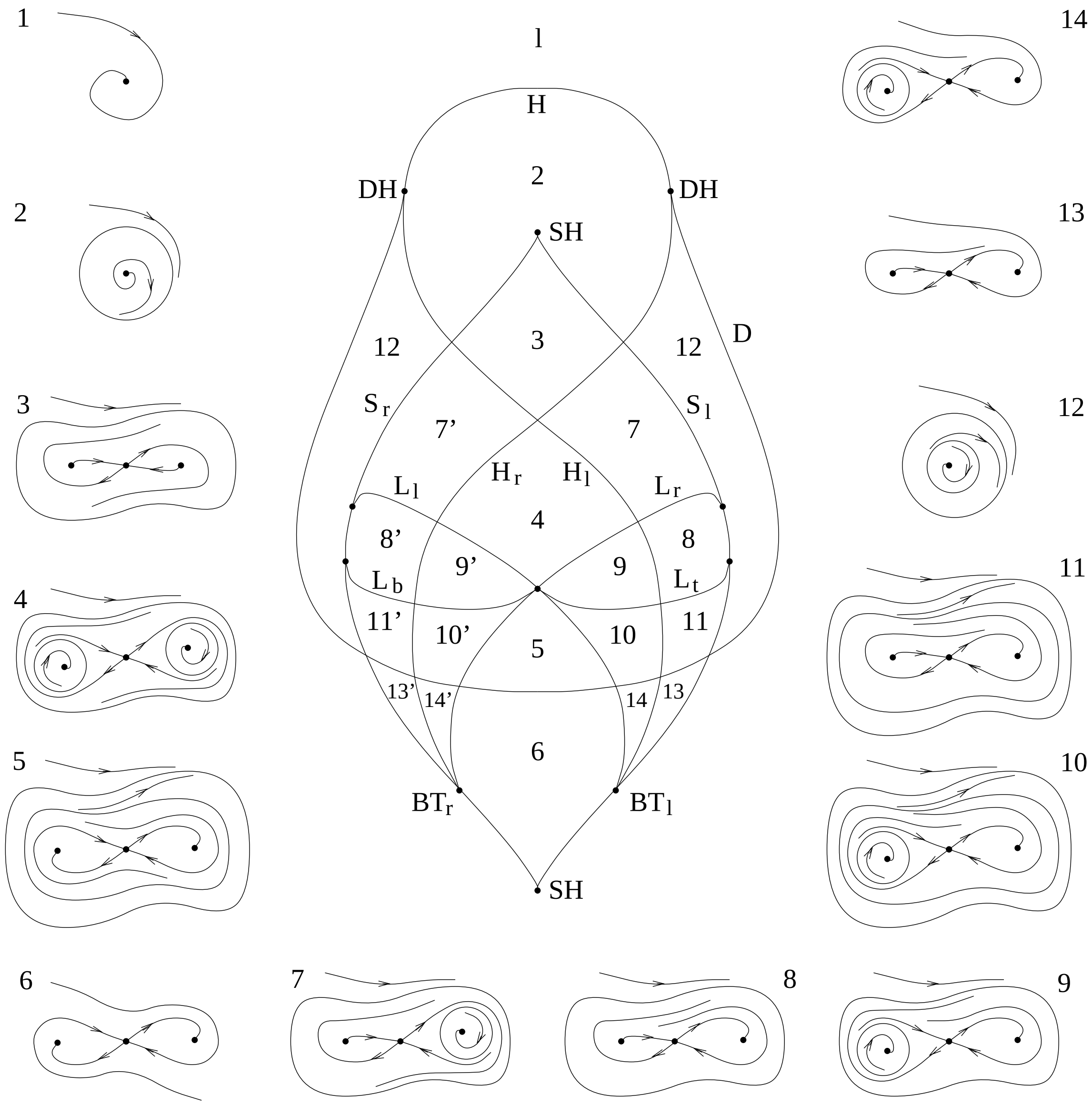

Figure 2: Sketch of the bifurcation diagram of (1.2) on a sphere around the singularity. The sphere minus one point is projected onto the plane. Adding or removing a prime corresponds to a rotation of the phase portrait by π.

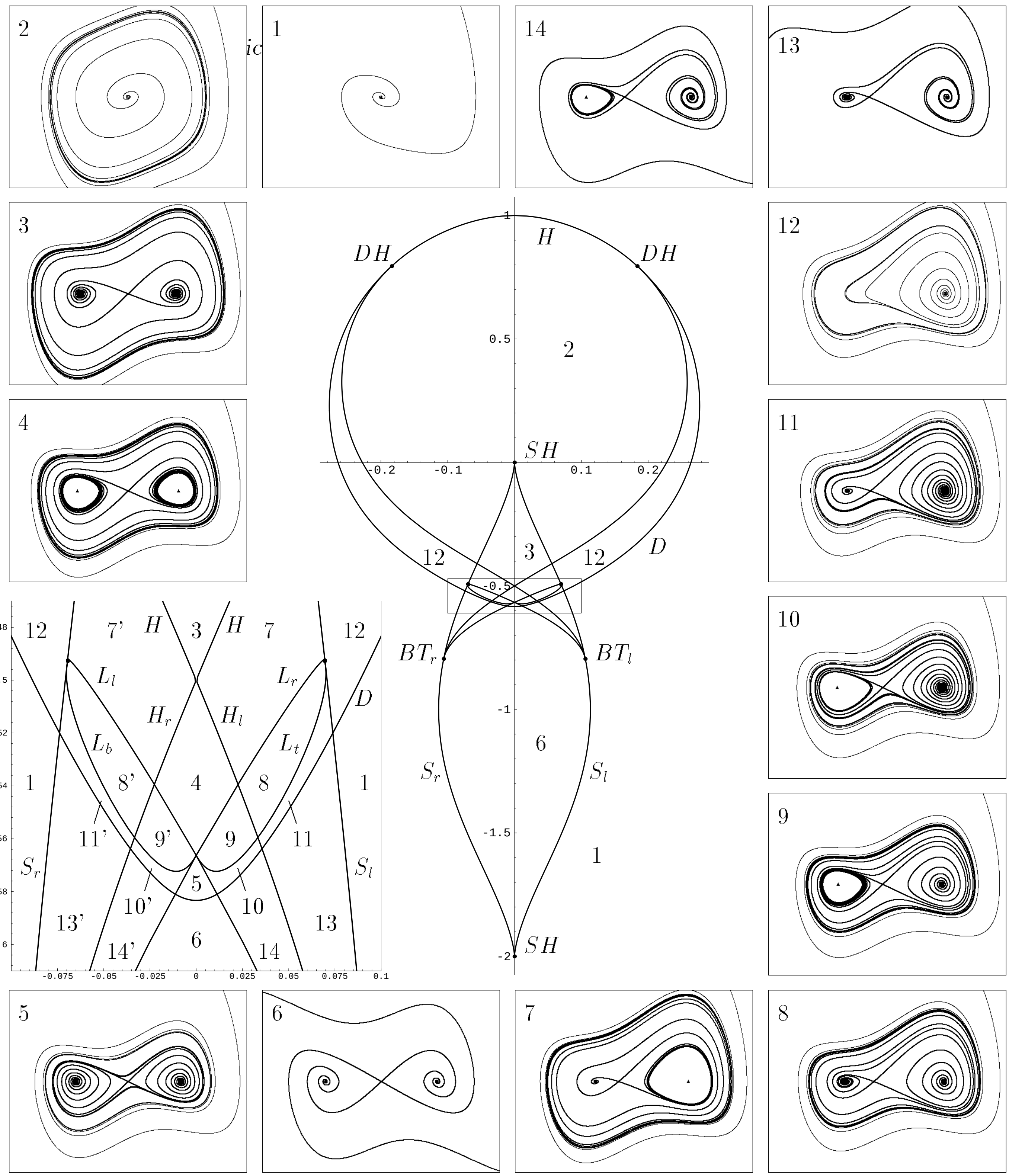

Figure 3: The bifurcation diagram of (1.2) on the unit sphere, projected onto the plane. Adding or removing a prime corresponds to a rotation of the phase portrait by π.

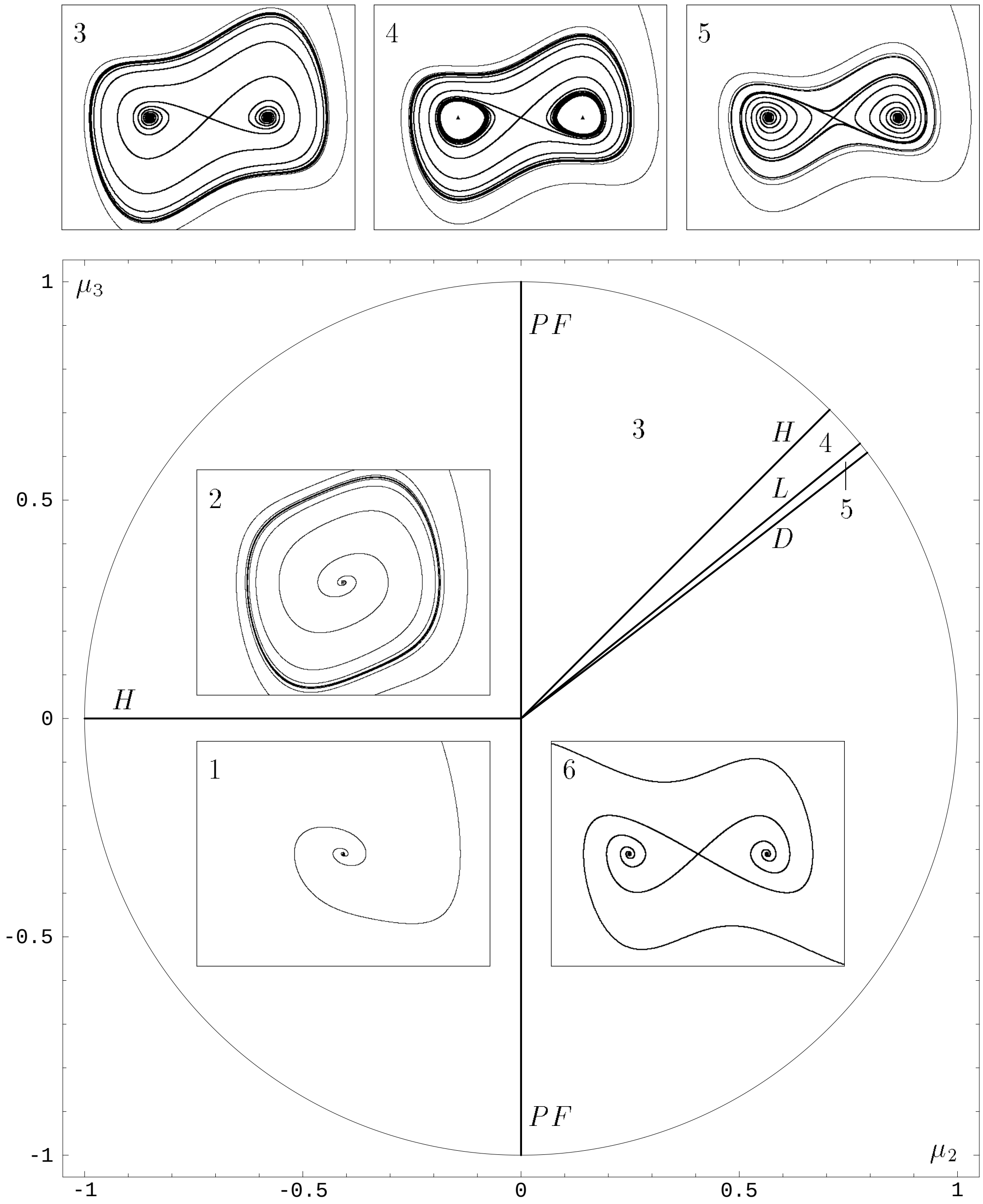

Figure 4: The $\mathbf{Z}_2$-equivariant unfolding for $\mu_1 = 0$.

The conic structure of the bifurcation diagram of (1.2) is not an a priori property. It rather follows a posteriori from the global knowledge of the bifurcation diagram. Indeed we study the intersections of the bifurcation diagram with nested spheres (or boxes) and show that they are all the same.

Equation (1.2) is a cubic Liénard equation, which has the general form

$$\begin{aligned} \dot{x} &= y \\ \dot{y} &= -g(x) - yf(x), \end{aligned} \tag{1.3}$$

where $f(x)$ is a polynomial of degree two, and $g(x)$ is a polynomial of degree three. Clearly, equation (1.2) is a particular case of a cubic Liénard equation with $f(x) = x^2 - \mu_3$ and $g(x) = x^3 - \mu_2 x - \mu_1$. System (1.3) is equivalent to the second order equation

$$\ddot{x} + f(x)\dot{x} + g(x) = 0, \tag{1.4}$$

which explains partly why the behaviour discussed here appears in so many models. There is a systematic approach to determine the maximum number of limit cycles of polynomial Liénard equations. Dumortier and Li [DL96] just finished the study of cubic equations with linear damping (the case $\deg(g) = 3$ and $\deg(f) = 1$) by filling the gap left in [DR90]. Our results are partial results in the general direction for $deg(g) = 3$ and $deg(f) = 2$. The theory allows us to use the powerful geometric methods introduced for Liénard equations, which are valid for all values of the parameters, and not just for small ones.

An equivalent of the family (1.2) has been studied intensively by Rychkov [Ry80, Ry84, Ry85] by combining the theory for Liénard equations with numerical methods. The geometry of the global bifurcation diagram is however missing in Rychkov's approach.

A candidate for a four-parameter unfolding of (1.1) is

$$\begin{aligned} \dot{x} &= y \\ \dot{y} &= \mu_1 + \mu_2 x + \mu_3 y + \mu_4 xy - x^3 - x^2 y \end{aligned} \tag{1.5}$$

which represents, when the μ_i are allowed to take arbitrary real values, the full family of cubic Liénard equations. In [DG87] a codimension-four family is studied that differs from (1.5) only in the quadratic term and contains implicitely (1.2) as a slice ($r = 0$ in the notation of [DG87]). But Figure 2 does not appear explicitely as a biproduct of the codimension 4 singularity in their work. Also, the study of the four-dimensional parameter space in [DG87] is in terms of small perturbations from a Hamiltonian system, where the term x^2y is small. Here we follow the idea of unfolding the central singularity (1.1) in a whole neighborhood. Our method is also valid for large μ_i and singular limits. Note that the motivation in [DG87] is similar to ours and see the references there for more examples from applications.

Obviously, the slice $\mu_4 = 0$ of the bifurcation diagram of (1.5) is the bifurcation diagram of (1.2) in Figure 2. For μ_4 sufficiently large the bifurcation diagram of (1.5) is in fact that of a nilpotent focus of codimension three [DRS91]. The full bifurcation diagram of (1.5) can be seen as the transition between the two. We present a conjecture of how we think this transition takes place. It involves passing through a cuspidal loop, a periodic orbit of multiplicity four (this periodic orbit of multiplicity four was not conjectured in [DG87], although it is implicit in their figures), and a cusp of order three.

This transition, given by the corresponding sequence of bifurcation diagrams, is complementary to the previous presentation of [DG87] and casts new light on this codimension-four bifurcation. A.D. Bazykin developed a similar transition in an unpublished paper in the 80's. Although he was not completely correct, he captured the major part of the transition.

To demonstrate our approach, we consider two models from applications in more detail: a quite general class of models, which includes the Bonhoeffer - van der Pol model [Gr87] and Bautin's model of electrical circuits in [Ba75], and an ecolocical model from [BBIK93]. We show how these models can be transformed to the form of (1.2) or to that of (1.5). Furthermore, we discuss certain singular limits of the models, which correspond to large (μ_1, μ_2, μ_3) in (1.2).

The paper is organized as follows. The main part is devoted to showing that the bifurcation diagram of (1.2) is as in Figure 2. In Section 2 we analyse the local bifurcations completely, and in Section 3 we study the global bifurcations, namely the different kinds of homoclinic connections and the double limit cycles. In Section 3.6 we discuss the completeness of the bifurcation set. In particular we address the question of its conic structure. The analytical results are complemented with the continuation of curves and surfaces of global bifurcation in Section 4. In Section 5 we indicate how the study here can be viewed as the starting point for studying the full four-parameter unfolding (1.5). Finally we discuss the mentioned models from applications in Section 6.

2 Local bifurcations

System (1.2) is symmetric under $(x, y, \mu_1, \mu_2, \mu_3) \mapsto (-x, -y, -\mu_1, \mu_2, \mu_3)$. In particular, it is sufficient to study the bifurcation diagram for $\mu_1 \geq 0$. We find the following local bifurcations in (1.2), which are shown in Figure 5; see also Figures 2 and 3.

Proposition 2.1
(a) There are two surfaces S_l and S_r of saddle-node bifurcations, given by

$$\Delta := 4\mu_2^3 - 27\mu_1^2 = 0. \tag{2.1}$$

For $\Delta < 0$ there is a unique equilibrium which is an antisaddle. For $\Delta > 0$ there are three equilibria , the middle point is a saddle, while the extreme points are antisaddles. On S_l the saddle-node bifurcation occurs on the left of the antisaddle, and on S_r it occurs on its right. At the line SH given by $\mu_1 = \mu_2 = 0$ there is a unique semi-hyperbolic node of codimension two.
(b) There is a surface H of Hopf bifurcations given by

$$P(\mu_3) := \mu_3^3 - 2\mu_3^2\mu_2 + \mu_3\mu_2^2 - \mu_1^2 = 0 \quad for \quad \mu_3 \geq \frac{\mu_2}{3}. \tag{2.2}$$

On the surface H there are two curves DH of degenerate Hopf bifurcations given by

$$\mu_2 + 3\mu_3 = 0 \quad and \quad 16\mu_3^3 - \mu_1^2 = 0. \tag{2.3}$$

For $\mu_2 + 3\mu_3 < 0$ the Hopf bifurcation is supercritical and for $\mu_2 + 3\mu_3 > 0$ it is subcritical. The degenerate Hopf bifurcation on DH is of order two, and in any perturbation the outermost limit cycle is stable.
(c) The intersection of H with S_l and S_r, respectively, defines two curves BT_l and BT_r of Bogdanov-Takens bifurcations, given by

$$\mu_2 - 3\mu_3 = 0 \quad and \quad 4\mu_2^3 - 27\mu_1^2 = 0. \tag{2.4}$$

The Bogdanov-Takens bifurcations generate repelling limit cycles.
(d) The surfaces and curves in (a)–(c) are invariant under

$$(\mu_1, \mu_2, \mu_3) \mapsto (\delta^3\mu_1, \delta^2\mu_2, \delta^2\mu_3)$$

for $\delta > 0$. Hence, they have conic structure, meaning that it is sufficient to consider their intersections with a sphere around the central singularity.

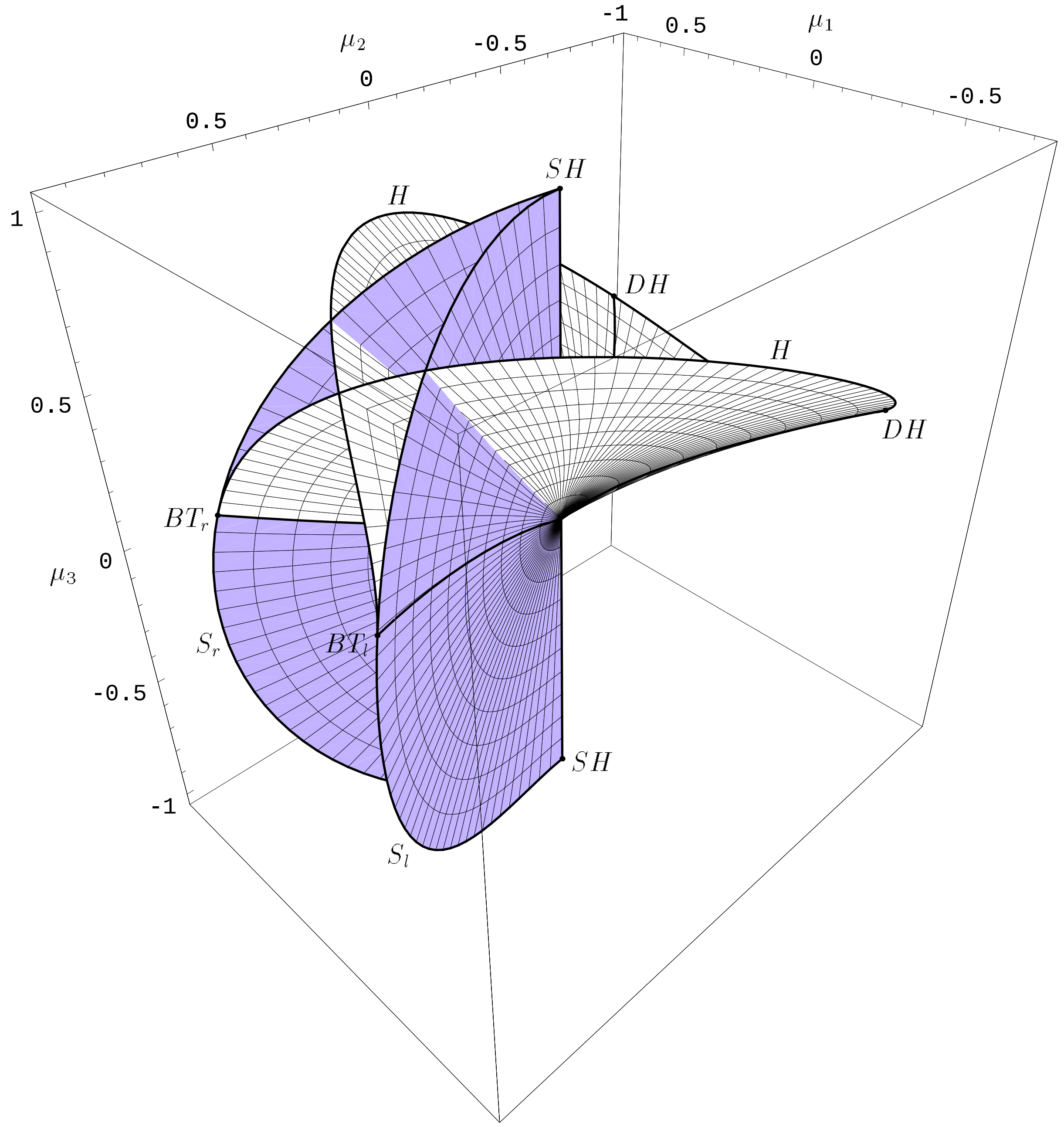

Figure 5: The saddle-node bifurcation surface (dark) with the curves of Bogdanov-Takens bifurcations, and the Hopf bifurcation surface (light) with the curves of double Hopf bifurcations, all inside the unit sphere.

Proof:
(a) The equilibria of (1.2) are given by $y = 0$ and $x^3 - \mu_2 x - \mu_1 = 0$, which has the discriminant $\Delta = 4\mu_2^3 - 27\mu_1^2$, and the result follows.

(b) A Hopf bifurcation can occur at an antisaddle when the divergence is zero there. The divergence is $div = -x^2 + \mu_3$, and it is zero for an x satisfying $x^3 - \mu_2 x - \mu_1 = 0$ exactly when $P(\mu_3) := \mu_3^3 - 2\mu_3^2\mu_2 + \mu_3\mu_2^2 - \mu_1^2 = 0$. Note that P is a cubic polynomial in μ_3 with polynomial coefficients in μ_1 and μ_2, and with discriminant $\mu_1^2(4\mu_2^3 - 27\mu_1^2)$, yielding three roots for P precisely when $\Delta > 0$ and $\mu_1 \neq 0$. The surface $P = 0$ has two upper leaves (in the region $\mu_3 > \frac{\mu_2}{3}$) that correspond to Hopf bifurcations at the left and at the right antisaddle. It also has a lower leaf (in the region $\mu_3 < \frac{\mu_2}{3}$) corresponding to a vanishing divergence at the saddle point. When $\mu_1 = 0$ and $\Delta > 0$, the surface has a self-intersection on the line $\mu_1 = 0, \mu_2 = \mu_3, \mu_2 > 0$ corresponding to simultaneous Hopf bifurcations at the two antisaddles (the system is symmetric for $\mu_1 = 0$). For $\Delta < 0$ the polynomial P has only one root. The line $\mu_1 = 0, \mu_2 = \mu_3, \mu_2 < 0$ also belongs to the manifold defined by $P = 0$. This line has no meaning for the bifurcation diagram of the real system. It corresponds to the simultaneous vanishing of the divergence at a pair of complex equilibria.

Now we study the type of the Hopf bifurcation. For this we localize the system at an antisaddle $x = x_0$, by means of the change of coordinates $X = x - x_0$. Then system (1.2) becomes

$$\begin{aligned}\dot{X} &= y\\ \dot{y} &= X(-3x_0^2 + \mu_2) - 3x_0X^2 - 2x_0Xy - X^3 - X^2y.\end{aligned}$$

We have a Hopf bifurcation if $\mu_2 - 3x_0^2 < 0$. We then let $y = -\sqrt{3x_0^2 - \mu_2}Y$ and divide the system by $\sqrt{3x_0^2 - \mu_2}$, yielding

$$\begin{aligned}\dot{X} &= -Y\\ \dot{Y} &= X + \frac{3x_0}{3x_0^2 - \mu_2}X^2 - \frac{2x_0}{\sqrt{3x_0^2 - \mu_2}}XY + \frac{X^3}{3x_0^2 - \mu_2} - \frac{X^2Y}{\sqrt{3x_0^2 - \mu_2}}.\end{aligned} \tag{2.5}$$

This system has the form

$$\begin{aligned}\dot{x} &= -y\\ \dot{y} &= x + a_{20}x^2 + a_{11}xy + a_{30}x^3 + a_{21}x^2y.\end{aligned}$$

For such a system the first two Poincaré-Lyapunov quantities are given by

$$\begin{array}{rcll} V_1 & = & \frac{1}{8}(a_{21} - a_{11}a_{20}) & \text{and} \\ V_2 & = & \frac{5}{48}a_{30}a_{11}a_{20} & \text{when } a_{21} = a_{11}a_{20}, \end{array} \tag{2.6}$$

which for (2.5) yields

$$V_1 = \frac{\mu_2 + 3\mu_3}{8(3x_0^2 - \mu_2)^{3/2}}.$$

Hence, the Hopf bifurcation is of order greater than one if $\mu_2 + 3\mu_3 = 0$ and of order one otherwise. For $V_1 = 0$ we get

$$V_2 = -\frac{5x_0^2}{(3x_0^2 - \mu_2)^{5/2}} < 0, \tag{2.7}$$

since for $x_0 = 0$ we have $\mu_1 = \mu_2 = 0$, that is, we have no longer a genuine Hopf bifurcation. This yields that the Hopf bifurcation is of order exactly two on the two curves given by (2.3). Moreover, according to (2.7) the weak focus of order two is stable and, hence, in any perturbation the outermost limit cycle is stable from the outside.

(c) Bogdanov-Takens bifurcations occur when the divergence vanishes at a double point, that is, when (2.1) and (2.2) hold simultaneously, which reduces to

$$\begin{array}{rcl} (4\mu_2 - 3\mu_3)(\mu_2 - 3\mu_3)^2 & = & 0 \\ 4\mu_2^3 - 27\mu_1^2 & = & 0. \end{array} \tag{2.8}$$

The curves $4\mu_2 = 3\mu_3, \Delta = 0$ correspond to a Hopf bifurcation at one equilibrium simultaneously with a saddle-node bifurcation of the other two. The curves $\mu_2 = 3\mu_3, \Delta = 0$ correspond to Bogdanov-Takens bifurcations. For $\mu_1 > 0$ the Bogdanov-Takens bifurcation occurs at the left equilibrium, and for $\mu_1 < 0$ it occurs at the right equilibrium. Localizing (1.2) at a Bogdanov-Takens point by means of $X = x - x_0$ yields

$$\begin{array}{rcl} \dot{X} & = & y \\ \dot{y} & = & -3x_0X^2 - 2x_0Xy - X^3 - X^2y, \end{array}$$

and consequently the Bogdanov-Takens bifurcations are always "repelling", meaning that they generate repelling limit cycles.

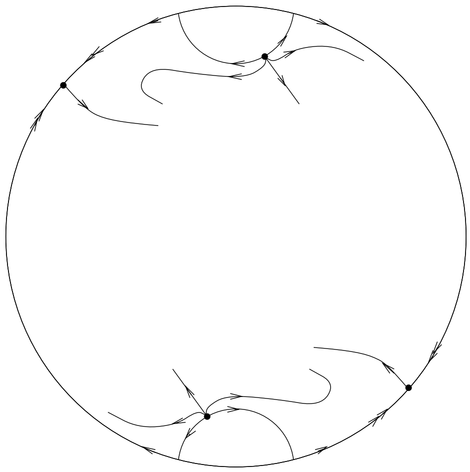

Figure 6: The blow-up at infinity on the Poincare disk.

(d) Follows immediately from the formulas. □

Since we are interested in the global unfolding of (1.2) we perform a study at infinity.

Proposition 2.2
For any value of (μ_1, μ_2, μ_2) the vector field (1.2) near infinity is as sketched on the Poincaré disk in Figure 6. In particular, infinity is always repelling.

Proof:
To study equilibria at infinity we pass to the coordinates $(v, z) = (x/y, 1/y)$. Then system (1.2), after multiplication by z^2, becomes

$$\begin{array}{rcl} \dot{v} & = & v^3 + v^4 + z^2 - \mu_3 v z^2 - \mu_2 v^2 z^2 - \mu_1 v z^3 \\ \dot{z} & = & v^2 z + v^3 z - \mu_3 z^3 - \mu_2 v z^3 - \mu_1 z^4. \end{array} \qquad (2.9)$$

The equilibrium at $v = -1$ is studied by means of the change of coordinates $V = v + 1$, transforming (2.9) into

$$\begin{array}{rcl} \dot{V} & = & -V + 3V^2 + (\mu_3 - \mu_2 + 1)z^2 - 3V^3 \\ & & +(2\mu_2 - \mu_3)Vz^2 + \mu_1 z^3 + O(|V, z|^4) \\ \dot{z} & = & Vz - 2V^2 z + (\mu_2 - \mu_3)z^3 + O(|V, z|^4). \end{array}$$

The center manifold is given by $V = (\mu_3 - \mu_2 + 1)z^2 + O(z^3)$, yielding

$$\dot{z} = z^3 + O(z^4),$$

along the center manifold. Hence, the equilibrium is a semi-hyperbolic saddle.

To study the equilibrium at $v = 0$ we use the weighted blow-up $(v, z) = (\pm\varepsilon^2, \varepsilon^3 Z)$. After division by ε^4 system (2.9) becomes

$$\begin{array}{rcl} \dot{\varepsilon} & = & \frac{1}{2}\varepsilon \pm \frac{1}{2}\varepsilon Z^2 + 0(\varepsilon) \\ \dot{Z} & = & -\frac{1}{2}Z \mp \frac{3}{2}Z^3 + O(\varepsilon), \end{array}$$

showing that all equilibria are repelling in the ε-direction. □

Remark 2.3 Proposition 2.2 gives us information on the parity of the number of limit cycles when $\Delta < 0$ and of the number of "large" limit cycles (surrounding all three singular points) when $\Delta > 0$. In the latter case this number is odd if the "object" formed by the separatrices of the saddle point is repelling, and even otherwise.

3 Global bifurcations

The aim of this section is to show that the global bifurcation curves D, L_l, L_r, L_t and L_b exist and are located in the bifurcation set of (1.2) as shown in Figure 2. The remaining questions about their exact positions are treated numerically in Section 4.

We know from Proposition 2.1(d) that the local bifurcations have conic structure. The global bifurcation curves and surfaces are associated with saddle connections and double limit cycles. For small μ_i's they are analysed below by transforming (1.2) to a near-Hamiltonian system. The bifurcation curves and surfaces are approximated by the parameter values where some elliptic integrals vanish, and the sets obtained consequently have conic structure. In the cases where the surfaces are not well-approximated by the near-Hamiltonian we used numerical methods to conclude that indeed the whole bifurcation set of (1.2) has conic structure; see Section 4.

As a consequence it is sufficient to present the intersection of the bifurcation set with a sphere, or for the purpose of this section, with a cube with faces parallel to the coordinate planes in (μ_1, μ_2, μ_3)-space. Considering a cube has the advantage that the vector field (1.2) has rotational properties on some of the faces of the cube.

For convenience we consider a cube with faces parallel to the coordinate planes where the edges where μ_1 and μ_2 are constant and $\mu_2 > 0$ are taken on $\Delta = 0$, that is, on S_l and S_r. The faces $\mu_3 = const$ are taken sufficiently small so that the bifurcation diagram consists only of $\Delta = 0$ and the phase portraits are known: on the lower face there is no limit cycle and on the upper face there is a unique "large" limit cycle. This comes from the knowledge of the phase portrait on the μ_3-axis and from the universality of the unfolding of the semi-hyperbolic node. It only remains to study what happens on the lateral faces. We have three equilibria on the front face and one on the three other lateral faces. The front face has several bifurcation curves. We use the following arguments.

(i) By studying the vector field along the μ_3-axis we find the bifurcation diagram on the faces $\mu_3 = const$.

(ii) We know the bifurcation diagram on the plane $\mu_1 = 0$ where the system is $\mathbf{Z}_2$-equivariant.

(iii) We give evidence for the bifurcation diagram along the edges of the cube where $\Delta = 0$.

(iv) By transforming the system to a near-Hamiltonian system the intersection of the front face of the cube with surfaces of saddle connections are approximated by graphs of functions $\mu_3 = \mu_3(\mu_1)$.

(v) For fixed values of μ_1 and μ_2 system (1.2) has rotational property When the parameter μ_3 is varied, which helps us in the study of the positions of the homoclinic loop curves and which yields unfoldings of double limit cycles.

Figure 2 is in fact the simplest possible picture taking into account all the information obtained in this section. In the next section we will focus on proving that there is nothing more.

3.1 The bifurcation diagram along the μ_3-axis.

Along the μ_3-axis the system has a unique equilibrium at the origin which is a semi-hyperbolic node (except for $\mu_3 = 0$). For $\mu_3 < 0$ the origin is attracting. Also the divergence does not vanish so that we have no limit cycle. For $\mu_3 > 0$ we necessarily have a limit cycle since the origin and infinity are both repelling. The fact that the system there has a unique hyperbolic limit cycle is proven exactly as for the van der Pol equation ([HS74] and Section 3.6) when one makes the change of coordinates $y = Y - \frac{1}{3}x^3 + \mu_3 x$, transforming (1.2), with $\mu_1 = \mu_2 = 0$, into

$$\begin{aligned} \dot{x} &= Y - \tfrac{1}{3}x^3 + \mu_3 x \\ \dot{Y} &= -x^3. \end{aligned} \tag{3.1}$$

3.2 The $\mathbf{Z}_2$-equivariant unfolding for $\mu_1 = 0$

For $\mu_1 = 0$ the system is symmetric with respect to the origin under the rotation by π. The remaining two-parameter family of planar vector fields is the well-known unfolding of a codimension-two nilpotent singularity of planar vector fields [Ca81, Kh85], the bifurcation diagram of which appears in Figure 4. In particular, for fixed $\mu_2 > 0$ and increasing μ_3 we cross the double limit cycle curve D first, then the double homoclinic curve L, and finally the Hopf bifurcation curve H. These crossings occur at $\mu_3 \approx 0.752\,\mu_2$ for the double limit cycle, at $\mu_3 \approx \frac{4}{5}\mu_2$ for the double homoclinic bifurcation, and at $\mu_3 = \mu_2$ for the Hopf bifurcation. Hence, we precisely know the bifurcation diagrams on the intersection of the plane $\{\mu_1 = 0\}$ with the cube.

3.3 The bifurcation diagram along $\Delta = 0$

Let us consider the edge of the cube $\mu_2 = C > 0$, $\mu_1 = \frac{2}{3\sqrt{3}}C^{\frac{3}{2}} > 0$, and let $c = \sqrt{C}$. Using the calculations in Proposition 2.1 we know that the system has two singular points, namely a double point located at $(x, y) = (x_0, 0) = (-c\frac{1}{\sqrt{3}}, 0)$ and a simple point at $(x, y) = (-2x_0, 0) = (c\frac{2}{\sqrt{3}}, 0)$.

The simple point is an anti-saddle. It is attracting for $\mu_3 < \frac{4C}{3}$ and repelling for $\mu_3 > \frac{4C}{3}$. At $\mu_3 = \frac{4C}{3}$ there is a subcritical Hopf bifurcation. The double point is a saddle-node for $\mu_3 \neq \frac{1}{3}\mu_2$ and a Bogdanov-Takens point for $\mu_3 = \frac{1}{3}\mu_2$. The saddle-node is attracting for $\mu_3 < \frac{1}{3}\mu_2$ and repelling for $\mu_3 > \frac{1}{3}\mu_2$.

We now determine the position of the separatrices of the double point; compare Figure 2. At the Bogdanov-Takens point BT_l the relative position of the separatrices is determined by the fact that the system has no limit cycle and that infinity is repelling (see Proposition 3.6 below). At the Hopf bifurcation H_r for the simple singular point the relative position of the separatrices is determined by the fact that the system has no limit cycle to the right of the saddle-node (see Proposition 3.8 below). Hence, between BT_l and H_r we need to have passed through a point L_r of right loop. A limit cycle appears there, which later disappears in the subcritical Hopf bifurcation H_r. By continuity we need to have a concave saddle connection L_t along the top of the equilibria between BT_l and L_r. Since the non-vanishing eigenvalue of the saddle-node is positive, passing through L_t when moving upwards leads to the disappearance of a large limit cycle. The only way a large limit cycle can have appeared between BT_l and L_t is through a multiple limit cycle bifurcation. The simplest such bifurcation is the saddle-node of limit cycle bifurcation D through the birth of a double limit cycle.

3.4 Reduction to a near-Hamiltonian system

We make the blow-up

$$\begin{array}{rclcrcl} x & = & \delta u & \qquad & \mu_1 & = & \delta^3\nu_1 \\ y & = & \delta^2 v & & \mu_2 & = & \delta^2\nu_2 \\ \tau & = & \delta t & & \mu_3 & = & \delta^2\nu_3, \end{array} \tag{3.2}$$

which transforms (1.2) into

$$\begin{array}{rcl} u' & = & v \\ v' & = & (-u^3 + \nu_1 + \nu_2 u) + \delta(\nu_3 v - u^2 v). \end{array} \tag{3.3}$$

This can be viewed as a small perturbation of the Hamiltonian system with Hamiltonian function

$$H(u,v) = \frac{v^2}{2} + \frac{u^4}{4} - \nu_1 u - \frac{\nu_2 u^2}{2}. \tag{3.4}$$

A necessary condition for limit cycles or homoclinic loops to appear for $\Delta \neq 0$ from closed ovals or homoclinic loops $\gamma(h)$ of $H = h$ is

$$M(h) = \oint_{\gamma(h)} (\nu_3 v - u^2 v)\, du = 0.$$

In the particular case of homoclinic loops, if $H = h_0$ is the singular curve of (3.4) when $\Delta \neq 0$ and $u_1 < u_2 < u_3$ are the intersection points of $H = h_0$ with the u-axis, then a necessary condition for the existence of a right homoclinic loop L_r is

$$M_r = \int_{u_2}^{u_3} (\nu_3 - u^2)(u - u_2)\sqrt{(u_3 - u)(u - u_1)}\, du = 0. \tag{3.5}$$

Similarly a necessary condition for the existence of a left homoclinic loop L_l is

$$M_l = \int_{u_1}^{u_2} (\nu_3 - u^2)(u_2 - u)\sqrt{(u_3 - u)(u - u_1)}\, du = 0, \tag{3.6}$$

and a necessary condition for a top or bottom concave homoclinic loop L_t or L_b is given by

$$M_c = \int_{u_1}^{u_3} (\nu_3 - u^2)|u - u_2|\sqrt{(u_3 - u)(u - u_1)}\, du = M_l + M_r = 0. \tag{3.7}$$

The vanishing of these functions obviously gives ν_3 as a function of ν_1 on a plane $\nu_2 = const$. Hence, on $\nu_2 = const$ the bifurcation curves of left, right and concave loops are approximated by graphs of functions $\nu_3 = \nu_3(\nu_1)$. These curves have a common point on $\nu_1 = 0$ and the relative positions of their end points on S_r and S_l are known. The simplest case is that these curves of homoclinic loops have no intersection points other than $\mu_1 = 0$. This is shown to be the case in the next section.

Note that the Hamiltonian approximation fails near the saddle-node bifurcations on S_r and S_l as the sum of the eigenvalues at a saddle-node is non-zero. It is an open question if and how the theory of perturbations from a hamiltonian can be modified to deal with global objects near saddle-nodes. For the time being numerical methods need to fill this gap.

For small values of the parameters we can prove that there is a unique intersection point of L_r and L_l by studying the appropriate abelian integrals for the near Hamiltonian system (3.3).

The formulas (3.5)-(3.7) give the locus of left, right or concave loops in terms of u_i. They can be calculated using symbolic manipulations. Since

$$(H-h_0)|_{v=0} = \frac{1}{/}4(u^4 - 2\nu_2 u^2 - 4\nu_1 u) = \frac{1}{4}(u-u_1)(u-u_2)^2(u-u_3),$$

we have that $u_2 = -\frac{1}{2}(u_1+u_3)$ and $u_1 < 0$, $u_3 > 0$. This helps to simplify the formulas.

Instead of giving the long formulas for M_r and M_l we only give the shorter ones for $M_c = M_l + M_r$ and $M_l - M_r$, from which they can be recovered.

$$\begin{aligned} M_l + M_r &= \tfrac{1}{32}(u_3-u_1)^2(u_3+u_1) \\ &\quad (-3u_1^2 - 2u_1u_3 - 3u_3^2 + 8\nu_3)\arcsin\tfrac{2(u_1+u_3)}{u_3-u_1} \\ &\quad + \tfrac{1}{1200}\sqrt{-(3u_1+u_3)(u_1+3u_3)} \\ &\quad (-9u_1^4 + 2u_1^2u_3^2 - 9u_3^4 + 10\nu_3(3u_1^2 + 2u_1u_3 + 3u_3^2)) \end{aligned}$$

and

$$M_l - M_r = \frac{\pi}{64}(u_3-u_1)^2(u_3+u_1)(3u_1^2 + 2u_1u_3 + 3u_3^2 - 8\nu_3).$$

Proposition 3.1
Except on S_l and S_r (where $\Delta = 0$) the equations of the bifurcation surfaces corresponding to left, right, top or bottom homoclinic loops are well approximated by the equations $M_l = 0$, $M_r = 0$ and $M_c = 0$. They correspond to generic bifurcations of saddle connections.

Proof:
The theory of saddle connections of a near-Hamiltonian system is well known; see for instance [Rou86]. The above equations lead to generic bifurcations if the trace at the saddle point is different from zero and the equations have a simple zero at that point. From the form of these equations which are linear in ν_3, with a non-vanishing coefficient of ν_3 (this requires a bit of work for the case $M_l = 0$), it is clear that the functions M_i have a simple zero when $\nu_3 = \nu_3(\nu_1)$. □

Proposition 3.2
The unique point of intersection of $M_l = 0$ and $M_r = 0$ in a plane $\nu_2 =$ const > 0 is located on ν_1=0. The slopes of the curves $M_l = 0$ and $M_r = 0$ at this point are given by $\frac{3\pi}{u_1}$ and $\frac{3\pi}{u_3}$, respectively.

Proof:
To find the intersection point of $M_l = 0$ and $M_r = 0$ we look at the system $M_l - M_r = M_l + M_r = 0$. The solutions of $M_l - M_r = 0$ are given by $u_1 + u_3 = 0$, which implies $u_2 = 0$ and we are on $\nu_1 = 0$ or

$$\nu_3 = \frac{1}{8}(3u_1^2 + 2u_1u_3 + 3u_3^2).$$

The solution $u_1 = u_3$ is excluded since u_1 and u_3 are of opposite signs. In the case $u_1 + u_3 = u_2 = 0$ we have that $M_r = M_l = 0$. This occurs when $\nu_1 = 0$ and

$$\nu_3 = \frac{2}{5}u_3^2 = \frac{4}{5}\nu_2.$$

Substituting this into $M_l + M_r = 0$ we obtain

$$\sqrt{-\frac{1}{4}(3u_1 + u_3)(u_1 + 3u_3)}(3u_1 + u_3)^2(u_1 + 3u_3)^2 = 0.$$

The solution $u_1 + 3u_3 = 0$ yields $u_2 = u_3$, that is, we are on L_r, while $3u_1 + u_3 = 0$ yields $u_1 = u_2$ and we are on L_l. The limiting position of the curve $M_c = 0$ and $M_r = 0$ as we approach S_l can be calculated by letting $u_3 \to -3u_1$, yielding

$$\nu_3 = \frac{1}{16}(7u_3^2 + 6u_3u_1 + 3u_1^2) = 3u_1^2 = \nu_2,$$

since $u_3 = -3u_2$ and $\nu_2 = 3u_2^2$. In first approximation, the homoclinic loop curves L_t and L_r cannot be distinguished on S_l. This has been observed numerically; see Section 4.

We now calculate the slope of the curve $M_r = 0$ at the point $\nu_1 = 0$, $\nu_3 = \frac{4}{5}\nu_2$. The slope of $M_l = 0$ at this same point is obtained using the symmmetry $(x, y, \nu_1, \nu_2, \nu_3) \mapsto (-x, -y, -\nu_1, \nu_2, \nu_3)$. This curve has an equation of the form $\nu_3 = M_3(\nu_1)$. The function $M_3(\nu_1)$ is obtained by solving $M_r = 0$, which is linear in ν_3. Its derivative is calculated as $\frac{\partial M_3}{\partial u_1}\frac{\partial u_1}{\partial \nu_1} + \frac{\partial M_3}{\partial u_3}\frac{\partial u_3}{\partial \nu_1}$. The quantities $\frac{\partial u_i}{\partial \nu_1}$ are obtained from the derivatives with respect to ν_1 of the equations

$$\begin{aligned}
\nu_1 &= \tfrac{1}{4}(u_1u_2^2 + u_2^2u_3 + 2u_1u_2u_3) = \tfrac{1}{16}(u_1 + u_3)(u_1 - u_3)^2 \\
\nu_2 &= \tfrac{1}{8}(3u_1^2 + 2u_1u_3 + 3u_3^2),
\end{aligned}$$

which yields

$$\begin{aligned} u_1' &= \frac{8}{(3u_1+u_3)(u_1-u_3)} \\ u_3' &= \frac{8}{(u_1+3u_3)(u_3-u_1)}. \end{aligned}$$

The expression $M_3'(\nu_1)$ has been calculated using Maple. It is long, but we only need to evaluate it at $\nu_1 = 0$, that is, for $u_1 + u_3 = 0$. This yields

$$M_3'(0) = \frac{3\pi}{u_3} = \frac{3\pi}{\sqrt{2\nu_2}}.$$

□

The necessary condition for a double limit cycle appearing from a closed curve of $H = h$ is given by $M(h) = M'(h) = 0$, and a sufficient condition is $M''(h) \neq 0$. If we let $I_i = \oint_{\gamma(h)} u^i v\, du$ then the necessary condition yields

$$\nu_3 I_0(h) - I_2(h) = \nu_3 I_0'(h) - I_2'(h) = 0, \tag{3.8}$$

where the $I_i(h)$ depend on ν_1 and ν_2. This holds for both, large limit cycles in the region with three singular points, and limit cycles in the region with one singular point.

Conjecture 3.3
We conjecture that (3.8) gives ν_3 as a function of ν_1 and ν_2. One way to prove this would be to show that the equation $K(h) = I_2(h)I_0'(h) - I_2'(h)I_0(h) = 0$ can be solved for $h = h(\nu_1, \nu_2)$. This would be the case if $K'(h) = I_2(h)I_0''(h) - I_2''(h)I_0(h) \neq 0$.

This conjecture is numerically confirmed in Section 4.

The information we have gathered so far is sufficient to conjecture that the bifurction diagram of (1.2) is as depicted in Figure 2. Additional evidence is given by the rotational property of the system.

3.5 Rotational property of the system

We consider system (1.2) for fixed values of μ_1 and μ_2. Then the system is a rotational family of vector fields [Du53, Pe75] with respect to the parameter μ_3. The rotational property gives for fixed μ_1, μ_2 and increasing μ_3 that repelling limit cycles decrease and attracting ones increase in size. Furthermore, double limit cycles that are attracting from the outside split into a pair of limit cycles. Finally, the separatrices of the saddle point move monotonously as μ_1 is fixed and μ_3 increases.

This helps us to determine what happens on the front face of the cube, in particular finding the positions of the homoclinic loop curves. The system is known for μ_3 sufficiently large since it is known on the horizontal edges. For fixed μ_1 and increasing μ_3 we either cross first the left homoclinic loop L_l, then the top homoclinic loop L_t and last the right homoclinic loop L_r, or else we cross first the right homoclinic loop L_r, then the bottom homoclinic loop L_b and last the left homoclinic loop L_l. A third possibility is that we have all loops simultaneously by crossing a single point corresponding to a figure-eight loop. Because of the rotational property we cross each saddle connection curve at most once on each line μ_1 constant. We know precisely what happens on the line $\mu_1 = 0$, since the system is symmetric there. In particular on this line all connections occur simultaneously, and we cross the curve of double limit cycles below the figure eight loop.

We now proceed by proving Proposition 3.6 and Proposition 3.8 that we already used in Section 3.3. The proofs rely on the fact that (1.2) is a Liénard equation, so that well-known criteria for Liénard equations can be applied to prove the non-existence of limit cycles, or the existence of a unique limit cycle. The proof of Proposition 3.1 uses the following criterion of Cherkas.

Theorem 3.4 (Cherkas [Ch77]) *Consider*

$$\begin{aligned} \dot{x} &= y - F(x)) \\ \dot{y} &= -g(x), \end{aligned} \tag{3.9}$$

where $xg(x) > 0$. If the system

$$\begin{aligned} F(x_1) &= F(x_2) \\ G(x_1) &= G(x_2), \end{aligned}$$

with $G(x) = \int_0^x g(\xi)\, d\xi$, has no solution in $\alpha < x_1 < 0 < x_2 < \beta$, then system (3.9) has no limit cycle in the region $\alpha < x < \beta$.

Idea of the proof:
We give the sketch of the proof since it also explains how to use the criterion in practice. The change of coordinates

$$X = X(x) = sgn(x)\sqrt{2G(x)},$$

together with the new time $T = t\ g(x)\frac{sgn(x)}{\sqrt{2G(x)}}$ transforms (3.9) into

$$\begin{aligned}\dot{X} &= y - F(x(X))\\ \dot{y} &= -X,\end{aligned}$$

where $x(X)$ is the inverse function of $X(x)$. The proof then goes on by comparing trajectories on the left and right side of $X = 0$ and uses differential inequalities ensuring that there cannot be closed loops. It requires no differentiability of the function $F(x(X))$. □

Remark 3.5 From the proof it is clear that the criterion is still valid under the weaker asumption $xg(x) \geq 0$ as long as equality only occurs at isolated points.

Proposition 3.6
There are no limit cycles at the Bogdanov-Takens points BT_l and BT_r.

Proof:
Because of the symmetry we can limit ourselves to the study of the Bogdanov-Takens bifurcation BT_l on the left, which occurs for $\mu_1 > 0$. Suppose the Bogdanov-Takens bifurcation takes place at a point $(x_0, 0)$, with $x_0 < 0$. Then

$$\begin{aligned}&x^3 - \mu_2 x - \mu_1 = (x - x_0)^2(x + 2x_0)\\ &x_0^2 - \mu_3 = 0.\end{aligned}$$

If we scale $x_0 = -1$ we get

$$\begin{aligned}\mu_1 &= -2x_0^3 = 2\\ \mu_2 &= 3x_0^2 = 3\\ \mu_3 &= x_0^2 = 1.\end{aligned}$$

We localize the system at $x = 2$, that is, we let $X = x - 2$, which gives

$$\begin{aligned}\dot{X} &= y\\ \dot{y} &= -X^3 - 6X^2 - 9X - y(X^2 + 4X + 3).\end{aligned}$$

We let $y = Y - (\frac{X^3}{3} + 2X^2 + 3X)$. This transforms the system into

$$\begin{aligned}\dot{X} &= Y - (\tfrac{X^3}{3} + 2X^2 + 3X) = Y - F(X)\\ \dot{Y} &= -X^3 - 6X^2 - 9X = -g(X).\end{aligned}$$

To be able to apply Cherkas criterion we need to proceed as in the proof above and make the change of variables

$$Z = Z(X) = \mathrm{sgn}(X)\sqrt{2G(X)},$$

where $G(X) = \int_0^X g(\xi)\, d\xi$ and $T = t\ g(X)\frac{\mathrm{sgn}(X)}{\sqrt{2G(X)}}$. Then the system becomes

$$\begin{aligned}\dot{Z} &= Y - F(X(Z))\\ \dot{Y} &= = -Z,\end{aligned}$$

where $X(Z)$ is the inverse function of the increasing function $Z(X)$. The final system is not C^1, but only continuous. This is sufficient to apply the criterion of Cherkas since

$$F(X) = \frac{X}{3}(X+3)^2 \begin{cases} > 0 & \text{for} \quad X > 0 \\ \leq 0 & \text{for} \quad X < 0. \end{cases} \tag{3.10}$$

Since $ZX(Z) > 0$ for $Z \neq 0$ we get the result by taking $\alpha = -\infty$ and $\beta = +\infty$. □

Our next result relies on the following Theorem of Zhang Zhifen.

Theorem 3.7 (Zhifen [Zh86])
Consider the system

$$\begin{aligned}\dot{x} &= y\\ \dot{y} &= -g(x) - f(x)y,\end{aligned} \tag{3.11}$$

satisfying $xg(x) > 0$ in an interval (α, β), $\alpha < 0$, $\beta > 0$. Then system (3.11) has at most one limit cycle for $x \in (\alpha, \beta)$ if the function $f(x)/g(x)$ is increasing or decreasing for $x \in (\alpha, \beta)$. Moreover, the limit cycle if it exists is attracting if $f(x)/g(x)$ is increasing and repelling if it is decreasing.

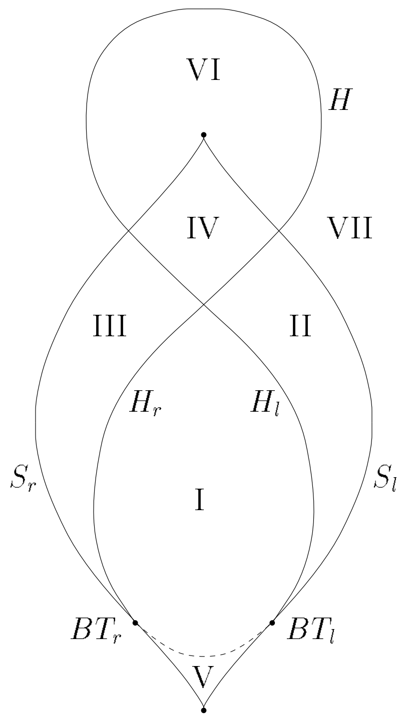

Figure 7: The regions of different limit cycles.

Proposition 3.8
Consider the regions depicted in Figure 7.

- *In region I there is at most one small limit cycle on the left and one small limit cycle on the right.*
- *In region II there is at most one small limit cycle on the right and no small limit cycle on the left.*
- *In region III there is at most one small limit cycle on the left and no small limit cycle on the right.*
- *In region IV there are no small limit cycles.*

In particular, there are no small limit cycles (surrounding only one equilibrium) at the intersection points of S_l with H_r and of S_r with H_l.

Proof:
We use Theorem 3.7 for our system which, localized at an equilibrium by means of $X = x - x_0$, has the form (3.11). In a region where we could have a small limit cycle we necessarily have that $Xg(X) > 0$ except at the equilibrium where it vanishes. The sign of the derivative of f/g can be calculated in the original x coordinate as

$$\left(\frac{f}{g}\right)' = -\frac{x^4 - (3\mu_3 - \mu_2)x^2 + 2\mu_1 x + \mu_2\mu_3}{g^2} = \frac{k}{g^2}.$$

The discriminant of k is given by

$$D_1 = 16[\mu_2(\mu_2 - 9\mu_3)^2 + 27\mu_1^2]P,$$

where P is given in (2.2). We discuss the different regions appearing in Figure 7. Since k has no roots in region I we conclude that in region I there is at most one small limit cycle on the left or on the right. In regions II (resp. III) the polynomial k has two roots. The resultant of k and g is

$$D_2 = \Delta P,$$

and since roots of k appear in pairs on the same side of the saddle. There are two roots of k on the left (resp. right) of the saddle point in region II (resp. III). We conclude that for $\mu_1 > 0$ (region II) there is at most one limit cycle on the right of the saddle point, and for $\mu_1 < 0$ (region III) there is at most one limit cycle on its right.

We can also conclude the non-existence of small limit cycles on the left in region II (on the right in region III) and on both sides in region IV (in which k has four real roots) by the argument below, together with the following remark. There can be no island containing an even number of limit cycles inside a region with no limit cycle for a rotational family. Indeed double limit cycles need to split when the rotational parameter varies [Pe75]. Hence, the leftmost and rightmost points of an island can only consist of points corresponding to multiple limit cycles of odd multiplicity. This is not possible since the island is located inside a region with no limit cycle.

Let us consider a plane $\mu_2 = const > 0$ and let us move up along lines $\mu_1 = const > 0$. In region I we have at most one limit cycle on the left and on the right. In region II we have at most one limit cycle on the right. When entering region II we cross a subcritical Hopf bifurcation on the left. Hence, we necessarily have no small limit cycle on the left at H_l and above in region II. A similar argument applies when we cross H_r and pass into region IV, yielding no limit cycle on the right on H_r and above. The argument works since we know that there is no small limit cycle for sufficiently large μ_3. □

Corollary 3.9
L_r cannot intersect H_r, and L_l cannot intersect H_l, except at the Bogdanov-Takens points.

Proof:
The Hopf bifurcations are subcritical and the divergence at the saddle point does not vanish on H. The existence of an intersection point would contradict the fact that the maximum number of small limit cycles on each side is one. □

Corollary 3.10
All intersections of L_r and L_l can only occur in region I.

Proof:
This is a consequence of the relative positions of these curves with respect to H_r and H_l. □

We have not been able to prove by techniques of Liénard equations and rotational properties alone that for all values of the parameters there is a unique curve corresponding to the intersection of L_r and L_l. This curve is located in the plane $\mu_1 = 0$ and corresponds to the figure-eight loop. For the moment we only have a proof for small values of μ_i as given in Section 3.4.

3.6 Conic structure of the bifurcation diagram

As mentioned in the introduction, the bifurcation diagram has conic structure, which comes a posteriori from the intersections of the bifurcation diagram with nested boxes. However, here again the part of the bifurcation diagram concerning double limit cycles is conjectural. The boxes are chosen as follows. They are symmetric with respect to each μ_i-axis and have vertical edges on the saddle-node surface $4\mu_2^3 - 27\mu_1^2 = 0$. This implies that the degenerate Hopf bifurcations occur on the lateral sides. On the bottom face there are no limit cycles since the divergence is negative. On the top face we show that there is exactly one limit cycle. This was already shown for the region with three singular points by Rychkov in [Ry85]. In the region with one singular point Rychkov proved in [Ry80] that there is exactly one hyperbolic limit cycle everywhere above the Hopf curve. The front and back faces lie in planes $\mu_2 = C$. On the back face we conjecture that the only bifurcation curve is the Hopf curve (which is supercritical). On the side faces lying in the planes $\mu_1 = C$ there are exactly two bifucation curves: the Hopf curve, and the curve of double limit cycles, which starts at the degenerate Hopf bifurcation and ends on the edge $4\mu_2^3 - 27\mu_1^2 = 0$. The front face contains the essentials of the dynamics. Rychkov [Ry85, Ry90] proved that there are at most two large limit cyles in the region with three singular points, which yields a maximal number of three limit cycles everywhere in that region. Using the rotational property with respect to μ_3 (which unfolds the semi-stable limit cycles) he concludes that in the case of two large limit cycles these are hyperbolic. His argument is not correct, since he does not exclude the case of multiple limit cycles of odd multiplicity. Hence, it is still a conjecture that, whenever there are two large limit cycles, then they are hyperbolic.

There are no limit cycles on the bottom face. If the box is sufficiently high then clearly there is exactly one hyperbolic limit cycle on the top face. The front face has been discussed in detail in Section 3.5 by using the rotational properties of the vector field with respect to μ_3. There the bifurcation diagram is complete up to the position of the double limit cycle curve. For the two sides faces and the back face the position of the double limit cycle curve is conjectural. We remark that we computed the double limit cycle curve by numerical methods; see Section 4. One way to prove the conjecture would be to show that double limit cycles occur on the front and back faces on a curve $\mu_3 = \mu_3(\mu_1)$ and on the lateral faces on a curve $\mu_3 = \mu_3(\mu_2)$, all these graphs yielding a global connected curve, as it is suggested by our computations. This conjecture may be attacked by means of elliptic integral in the case of small values of the parameters. Because of the rotational property with respect to μ_3, to prove the conjecture it suffices to prove that the system has no triple limit cycle.

4 Numerical methods

Numerical techniques make it possible to give evidence for conjectures one may be unable to prove. Furthermore, it is generally very interesting to see how the qualitative picture manifests itself quantitatively in a given system. Another attractive feature is to combine numerical methods with visualization tools. It is obvious that it is difficult to convey on paper the intricate structure of a bifurcation diagram in a three-dimensional parameter space. This is why we have installed a 3D-viewer and a movie providing extra illustration of the bifurcation set of (1.2) in color. The reader is encouraged to visit `http:www.nat.vu.nl/~berndk/kkr/kkr.html` and explore the bifurcation set interactively.

To consider the intersection of the bifurcation diagram of (1.2) with a sphere we use the parametrization

$$\begin{aligned} \mu_1 &= r\sin(\pi\alpha) \\ \mu_2 &= -r\cos(\pi\alpha)\sin(\frac{\pi}{2}\beta) \\ \mu_3 &= r\cos(\pi\alpha)\cos(\frac{\pi}{2}\beta). \end{aligned} \tag{4.1}$$

This choice is convenient, and we are interested in the bifurcation diagram in the (α,β)-plane for fixed r, where $-\frac{1}{2} \leq \alpha \leq \frac{1}{2}$ and $-2.5 < \beta < 1.5$. Clearly, this projection can be used to draw the intersection of the bifurcation diagram with the unit sphere $\mu_1^2 + \mu_2^2 + \mu_3^2 = 1$ simply by fixing $r = 1$. The local bifurcation curves can be calculated from their parametrizations in Proposition 2.1. The global curves were calculated by continuation with the continuation package `AUTO` [DK86] in combination with the driver `HomCont` [CKS95] for the calculation of homoclinic connections.

To calculate the curve D of double limit cycles we used `AUTO` to follow the fold curve of limit cycles for fixed $r = 1$ in the (α,β)-plane. We started the calculation at the symmetric case for $\alpha = 0$ and calculated the curve D for positive α as far as possible. The endpoint that `AUTO` found is very close to the point DH given by Proposition 2.1(b). The other half of D can be obtained by the symmetry $\alpha \mapsto -\alpha$.

For the calculation of the different curves of homoclinic loops we used `HomCont`. Again because of symmetry we calculated only L_r and L_t. To start the calculation we first found the figure-eight loop in the symmetry

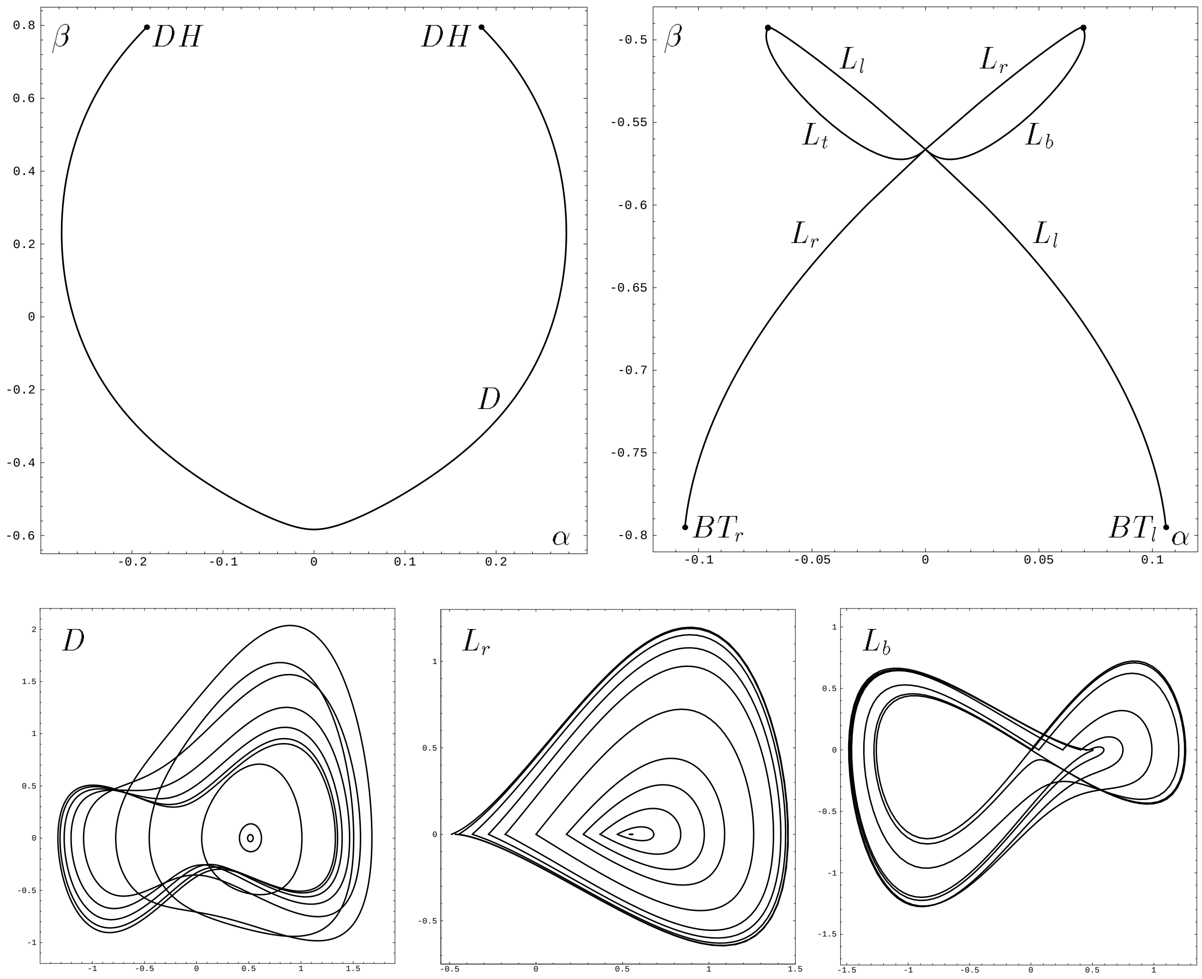

Figure 8: Top: The global bifurcation curves D of semistable limit cycles (left), and L_r, L_l, L_b and L_t of homoclinic loops (right). Bottom: Objects along the global bifurcation curves: semistable limit cycles along D for $\mu_2 \geq 0$ (left), small homoclinic loops along L_r (middle), and big homoclinic loops along L_b (right).

plane $\alpha = 0$ by homotopy [DFM93]. The figure-eight contains in particular a right homoclinic loop and the calculation of L_r can be started from there: for positive α until S_l is reached, and for negative α until BT_r on S_r is reached. Note that `HomCont`, or rather the boundary-value solver of `AUTO`, runs into convergence problems close to the saddle-node curves S_l and S_r. Nevertheless, one typically gets very close to these curves.

The bifurcation diagram of the $\mathbf{Z}_2$-equivariant unfolding for $\mu_1 = 0$ in Figure 4 is also quantitative. We calculated D and L_r for fixed $\alpha = 0$ and $r \to 0$ to obtain data that was then transformed to the (μ_1, μ_2)-plane by using (4.1).

The calculation of L_t cannot be started from the figure-eight, but a different starting point must be found by homotopy. We used a point close to the figure-eight for small positive α. From there L_t can be continued in both directions, to the intersection point with the symmetry line $\alpha = 0$, and until S_l is reached. Note that for small α the concave homoclinic loop on L_t passes extremely close to the saddle point, leading to convergence problems. However, for suitable choices of the internal constants of `HomCont` one can practically find all of the curves L_r and L_t.

The results of our calculations of the global bifurcation curves are summarized in Figure 8 showing the global curves in the (α, β)-plane, together with some snapshots of the respective objects that have been continued. The complete bifurcation diagram is shown in Figure 3. The enlargement of the box near the intersection point of L_l and L_r (corresponding to the figure-eight) is included to clearly show the relative positions of the bifurcation curves. There is a total of 14 topologically different phase portraits, representatives of which are shown as panels obtained with `DsTool` [BGMWW92]. The rotation of a phase portrait by π corresponds to attaching or removing a prime.

Figure 3 is clearly in agreement with the topological nature of Figure 2. We remark that it is known that there is a tangency between L_r and S_l and between L_l and S_r, as it is sketched in Figure 2. However, this is not visible when the the curves L_r and L_l are numerically computed, as they seem to approach S_l and S_r in an angle, and then turn around the corner very sharply. Note that the endpoints of the curves L_r and L_t on S_l and of L_l and L_b on S_r are indistinguishable in Figure 3. Numerically, this distance is less than $2 * 10^{-4}$. This illustrates the result in the proof of Proposition 3.2 that these endpoints are in fact identical in first approximation.

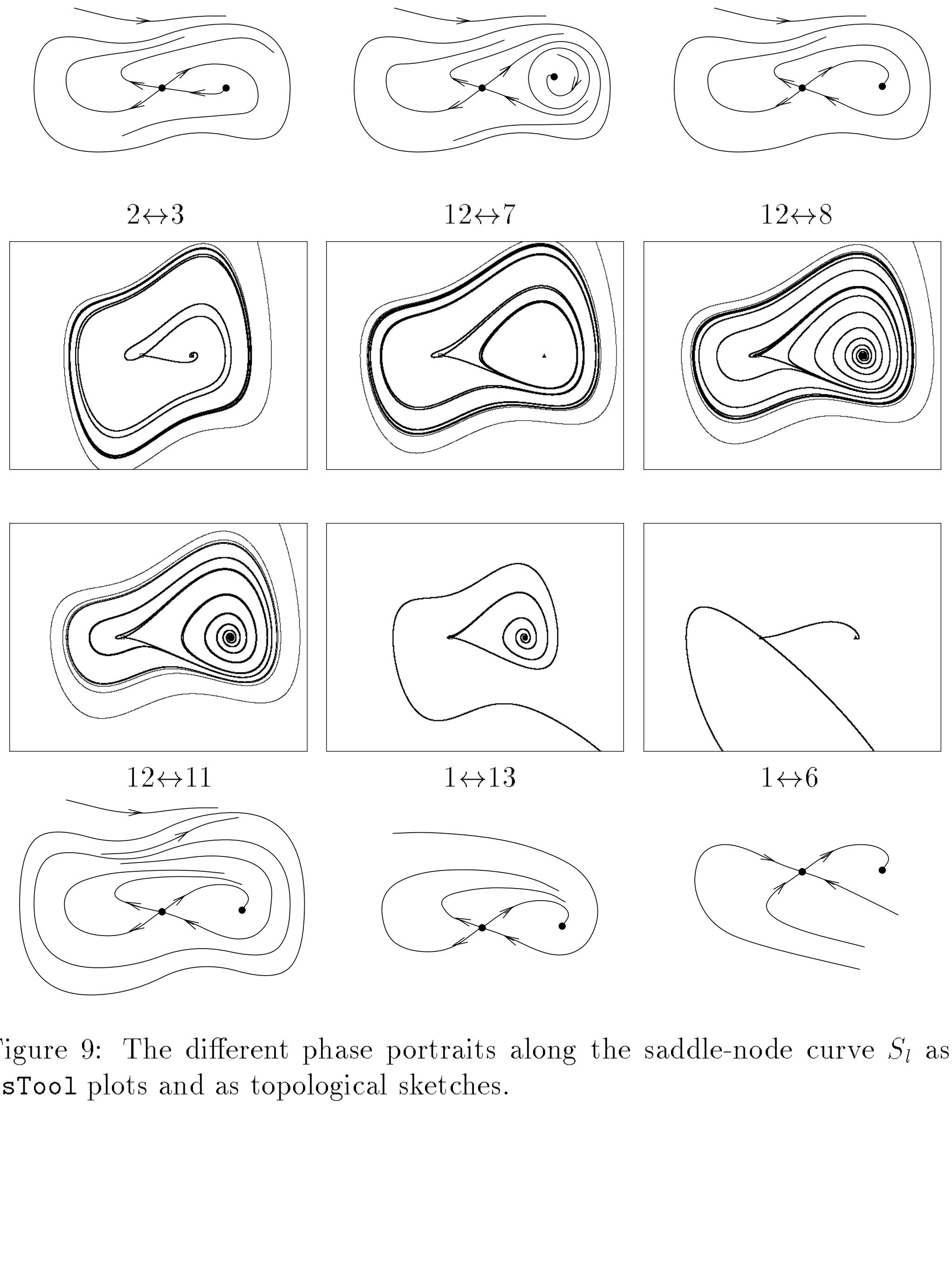

Figure 9: The different phase portraits along the saddle-node curve S_l as `DsTool` plots and as topological sketches.

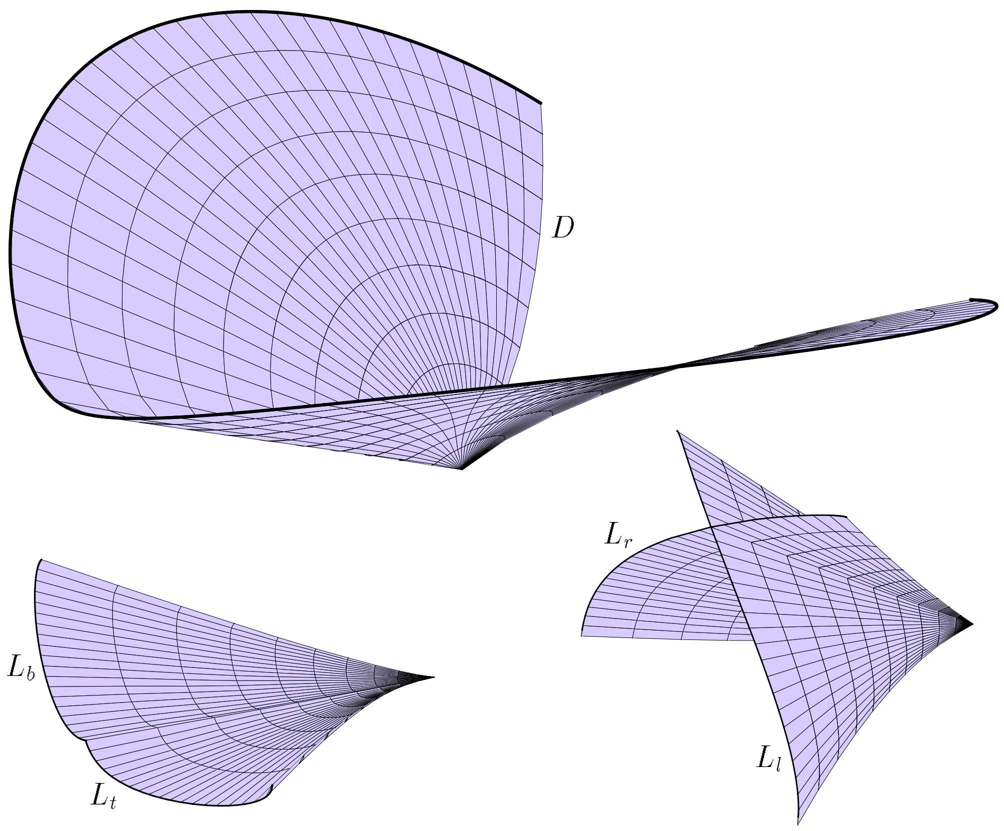

Figure 10: The global surfaces inside the unit sphere as computed with `HomCont/AUTO`.

That they cannot coincide follows from topological arguments, but can also be checked numerically. Figure 9 shows the phase portraits of generic saddle-node bifurcations along S_l, both as topological sketches and as `DsTool` panels. The presence of the panel $12 \leftrightarrow 8$ shows that L_r and L_t indeed end at different points on S_l. Note that the two unstable manifolds of the saddle-node are very close together. Consequently, the two parameter values for which one of the two stable manifolds coincides with the neutral stable direction (the endpoints of L_r and L_t) are extremely close together.

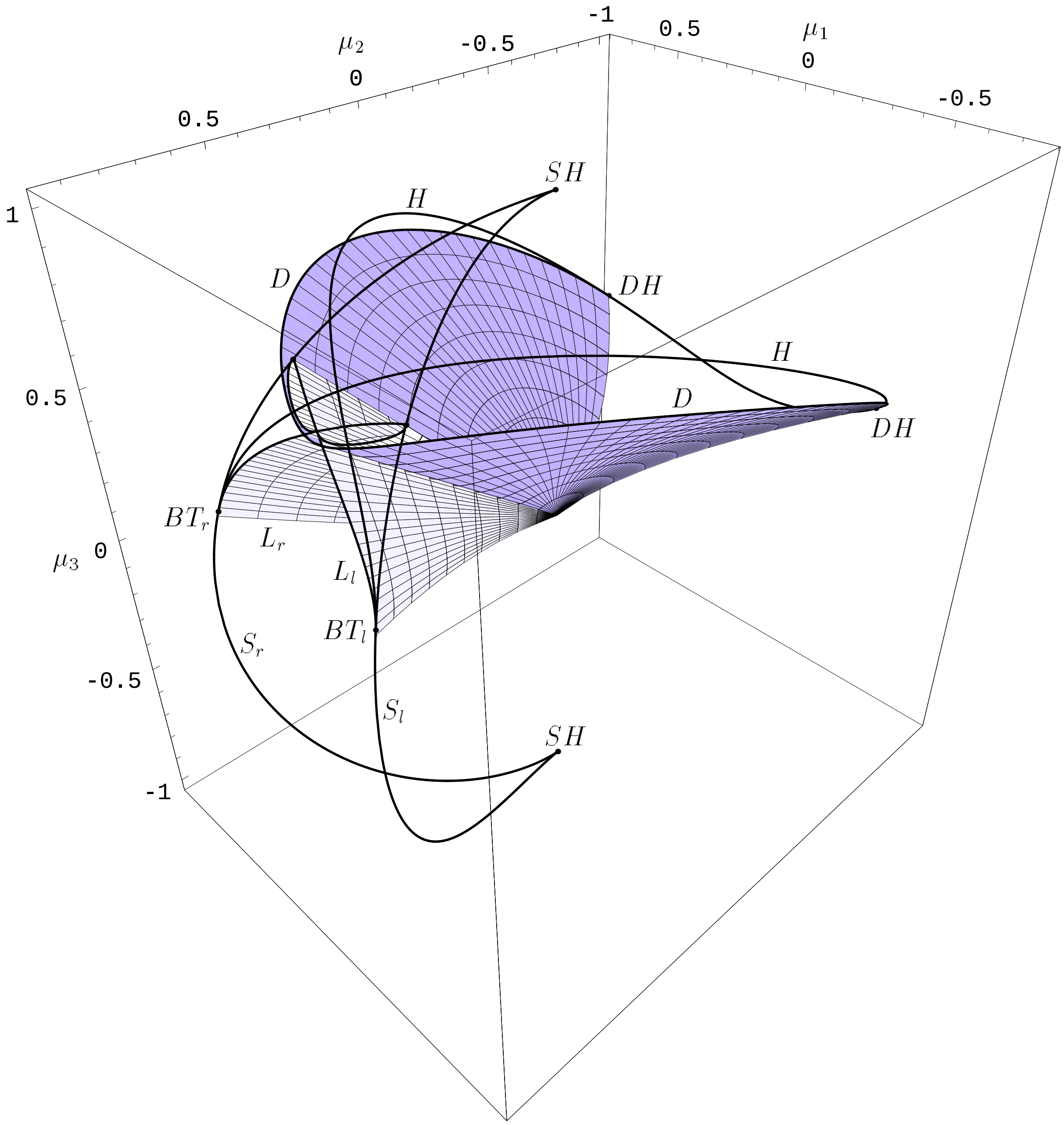

Figure 11: The bifurcation set on the unit sphere with the surfaces of global bifurcations inside it.

As evidence that the surfaces of global connections have conic structure we calculated them. To do this we continued the respective curves in the (α, β)-plane for the values $0.1, 0.2, \ldots, 1.0$ of the radius. This allowed us to construct the global surfaces in (μ_1, μ_2, μ_3)-space as is shown in Figure 10. In particular, these calculations confirm the conjecture that the μ_3-value of the surface D is a function over the base (μ_1, μ_2).

The results of the different computations are combined in Figure 11. It shows all bifurcation curves *on* the unit sphere (which is not shown) in (μ_1, μ_2, μ_3)-space, together with the global surfaces *inside* the unit sphere. Figure 11 should be compared with Figures 3 and 8, and with the local surfaces in Figure 5.

5 The codimension-four unfolding

In this section we briefly describe what we think the full unfolding of (1.5) looks like. It can be described as a transition from the bifurcation diagram of (1.2) by letting μ_4 increase from 0 to $+\infty$; see Conjecture 5.1 below. In (1.5) and in this transition several codimension-three bifurcations occur, namely

1. local bifurcations, that is, bifurcations of singular points,
2. bifurcations involving saddle connections, and
3. bifurcations of multiple limit cycles.

Among the local bifurcations there is the cusp of order three and the nilpotent focus. Also, several global bifurcations of codimension three appear in (1.5). To be more concrete, we expect the following codimension-three bifurcations to occur in the transition. (The capital letters refer to the bifurcation diagrams in Figure 12.)

Sequence of codimension-three bifurcations

- a double limit cycle simultaneously with a Bogdanov-Takens bifurcation; between A and B.
- a cuspidal loop when the separatrices of a Bogdanov-Takens point form a loop (we prove below that this bifurcation indeed occurs); at C between B and D.

- a limit cycle of multiplicity four with its generic unfolding given by the swallow tail. The limit cycle of multiplicity four is the new feature of our approach. It occurs at F, between E and G.
- a bifurcation of simultaneous Hopf and Bogdanov-Takens bifurcations, given as the intersection of H_r and BT_l; between G and H.
- a degenerate Hopf bifurcation H_r together with a saddle-node on the left; between H and I.
- a cusp of order three; between I and K.
- a bottom homoclinic loop of order three; between L and M.
- finally, for large μ_4 the bifurcation diagram is the same as for the nilpotent focus; see M and compare [DRS91].

All of these bifurcations had been explicitely noticed in [DG87], except for the limit cycle of multiplicity four, although it seems natural to conclude that it exists from case A of Fig.2c–g of [DG87]. There the curve of double limit cycles has self-intersections as in a cross-section of the swallow tail. Indeed a curve of triple limit cycles should appear in the bottom homoclinic loop bifurcation of order three, and another one appears in the unfolding of the cuspidal loop. To prove that the triple limit cycle appearing from the bottom homoclinic loop of order three is attracting we need to prove that the first saddle quantity is negative at the moment when the loop exists. In practice we can calculate the first saddle quantity, but to determine its sign we need to know the parameter values for which the loop occurs. On the other hand, the triple limit cycle is repelling near the cuspidal loop. If these two curves were the two ends of a connected curve of triple limit cycles, then this curve would need to pass through a point corresponding to a limit cycle of multiplicity four. An associated region with four limit cycles was indeed found in [DG87]. In [Ma94] it has been proved (with rigorous numerics) that there are indeed four limit cycles in (1.5). The region with four limit cycles was found to be extremely narrow; see [Ma94] for details.

We now come to a more detailed description of the codimension-four unfolding given by (1.5). The bifurcations of equilibria occur on sets invariant under

$$(\mu_1, \mu_2, \mu_3, \mu_4) \mapsto (\delta^3\mu_1, \delta^2\mu_2, \delta^2\mu_3, \delta\mu_4), \tag{5.1}$$

yielding conic structure of these surfaces. We conjecture that the whole bifurcation set of (1.5) has conic structure for small values of the parameters. This allows us to consider the intersection of the bifurcation diagram of (1.5) with a cube in $(\mu_1, \mu_2, \mu_3, \mu_4)$-space, whose faces are parallel to the coordinate hyperplanes $|\mu_i| = C_i$.

The system is invariant under $(x, y, \mu_1, \mu_4) \mapsto (-x, -y, -\mu_1, -\mu_4)$, so that we may take $\mu_4 \geq 0$. We now think of this cube as the family of its intersections with hyperplanes of the form $\mu_4 = C$, with $C \geq 0$. If C is close to zero we get in (μ_1, μ_2, μ_3)-space the bifurcation set of (1.2) of Figure 3. On the other hand, if C is very large (with respect to the other C_i) then we get the bifurcation diagram of the nilpotent cusp of order three. This bifurcation diagram is known to have conic structure; see [BKK85] and [DRS91] and case (M) of Figure 12. By varying C we find a transition of the bifurcation diagram of (1.2) to that of the nilpotent cusp of order three. Each bifurcation diagram in the transition can be illustrated by its intersection with a sphere in (μ_1, μ_2, μ_3)-space.

Conjecture 5.1
The unfolding in $(\mu_1, \mu_2, \mu_3, \mu_4)$-space of (1.5) is given by the transition of the bifurcation set in hyperplanes $\mu_4 = C$ from $C = 0$ to C (sufficiently) large, as sketched in Figures 12 with the associated phase portraits in Figure 13. It has conic structure for small values of the parameters.

The transition shown in Figure 12 constitutes the simplest topological model of the unfolding of (1.5) when all information is taken into account. By increasing μ_4 one passes through the sequence of bifurcations presented above. We remark that in Figure 12 we do not give all topologically different bifurcation sets on a sphere in (μ_1, μ_2, μ_3)-space, but concentrate on the important ones that were just mentioned. The reader is encouraged to interpolate the transition between the panels of Figure 12 where necessary.

We finish this section by showing that most of the bifurcations listed in the sequence of codimension-three bifurcations indeed appear in that order. What is not proved here remains conjectural and will be studied elsewhere. In particular, we prove that the cuspidal loop does exist, and determine its type.

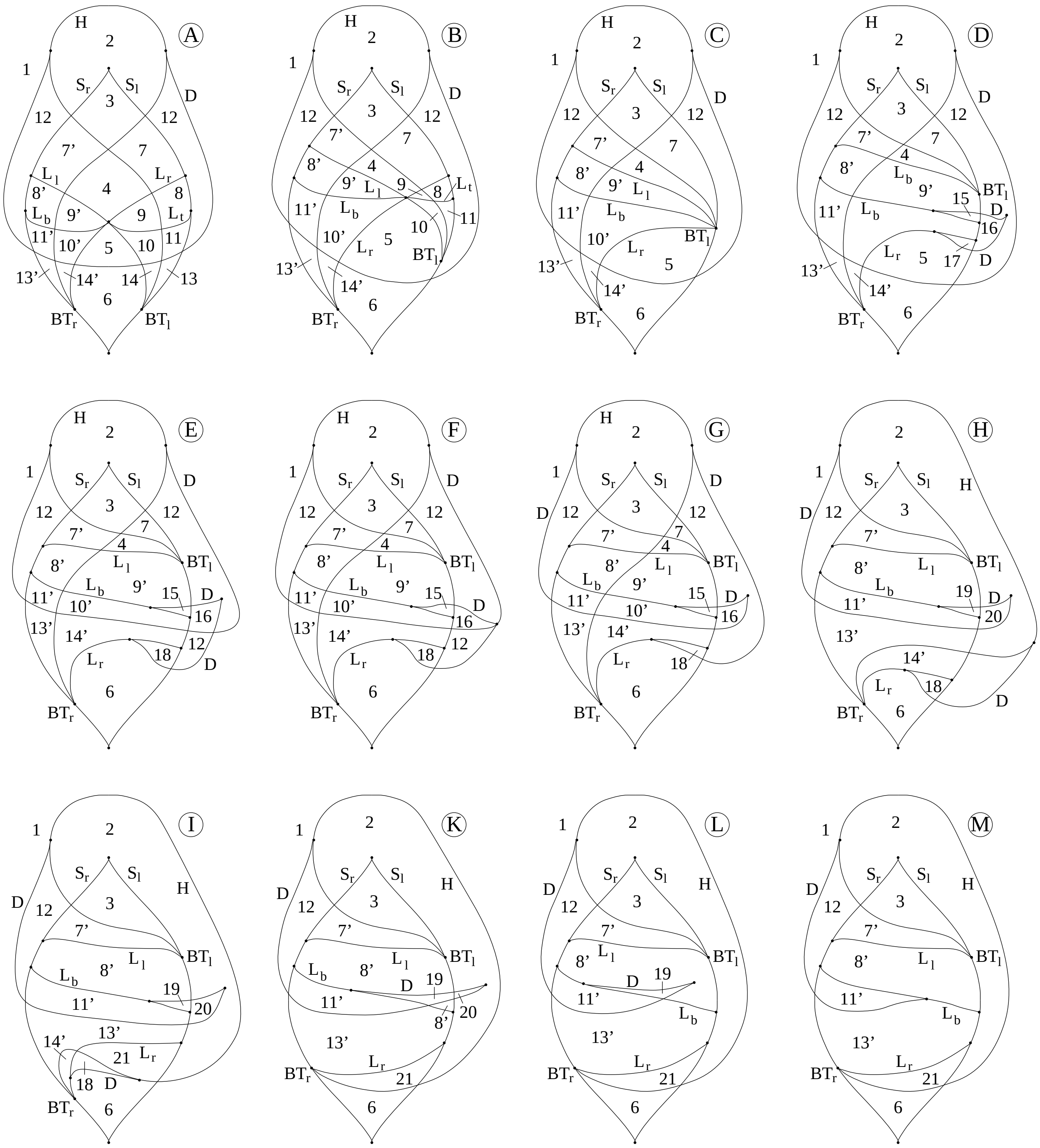

Figure 12: Sketch of the transition from $\mu_4 = 0$ to $\mu_4 \gg 0$.

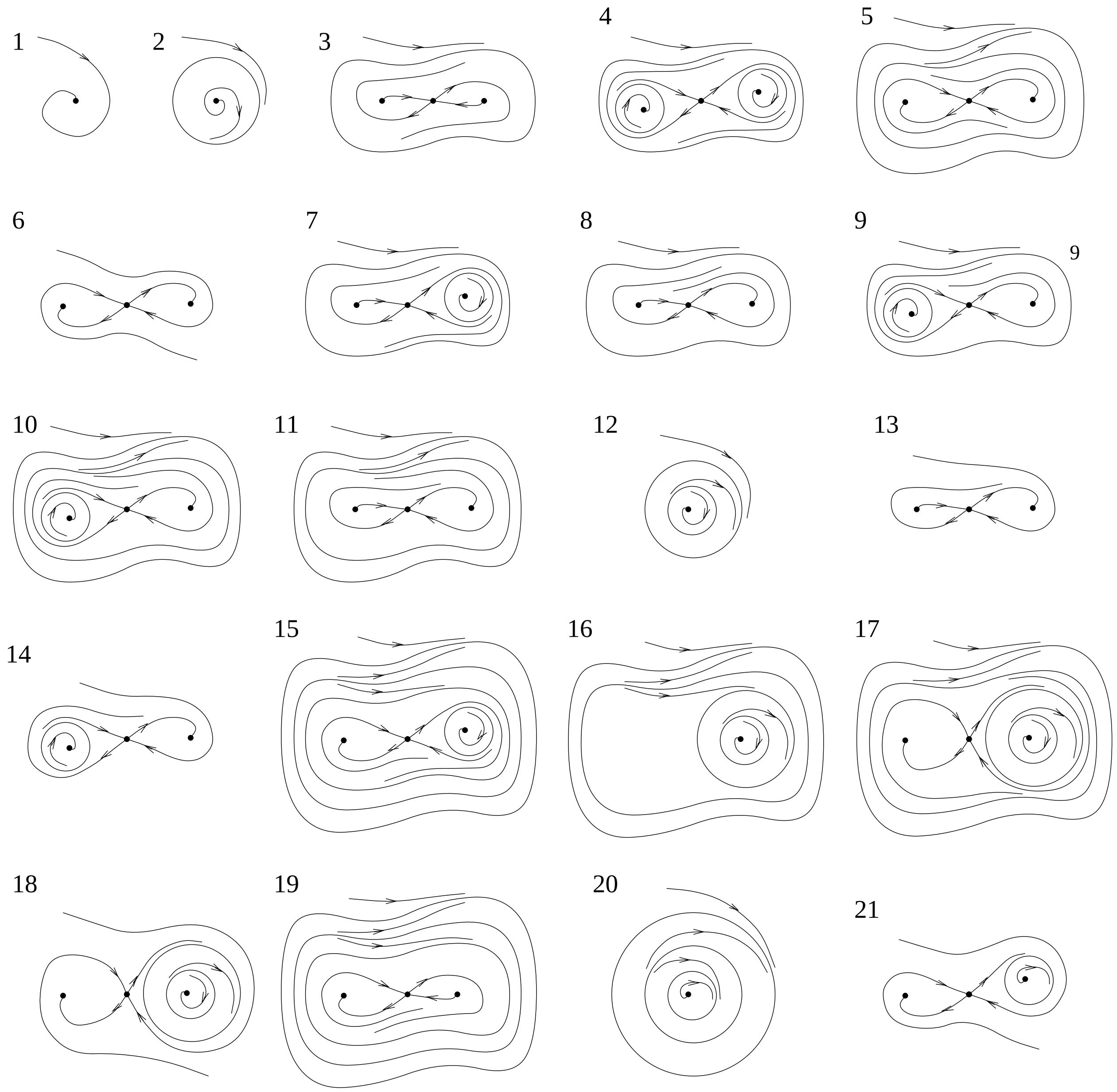

Figure 13: The 21 phase portraits appearing in the transition in Figure 12.

After we finished this paper we learned that the existence of the cuspidal loop and of the sequence of bifurcations for the subfamily with a Bogdanov-Takens point had been studied in [WK92]. Since our proof is simple we included it for the sake of completeness, instead of calculating the transformation of our system to the form in [WK92].

Proposition 5.2
There exists a positive value of μ_4 for which the system has a repelling cuspidal loop attached to a Bogdanov-Takens point located on the left (at C *between* B *and* D*).*

Proof: System (1.5) has a Bogdanov-Takens point at x_0 if $x^3 - \mu_2 x - \mu_1 = (x-x_0)^2(x+2x_0)$ together with $\mu_3 = x_0^2 - \mu_4 x_0$; compare Theorem 2.1(c). In Proposition 3.6 we have shown that there are no limit cycles at the moment of the Bogdanov-Takens bifurcation for $\mu_4 = 0$. Let us consider a bifurcation on the left and suppose that $x_0 < 0$. Then the system has a Hopf bifurcation at $x = -2x_0 > 0$ for $\mu_4 = -x_0$. The first Lyapunov quantity being positive, the bifurcation creates a repelling limit cycle when the point is attracting, that is, when $\mu_4 < -x_0$. At the Hopf bifurcation the system needs to have an attracting limit cycle, since the weak focus and infinity are both repelling.

We now show that for $\mu_4 \in [0, -x_0]$ there is no small attracting limit cycle, so that the attracting limit cycle present at the moment of the Hopf bifurcation must be large. We localize system (1.5) at the weak focus by means of $X = x + 2x_0$ and obtain

$$\begin{aligned} \dot{X} &= y \\ \dot{y} &= -X(X-3x_0)^2 - 3x_0(x_0+\mu_4)y + (\mu_4+4x_0)Xy - X^2y. \end{aligned}$$

We now use Theorem 3.7 to the right of x_0. Indeed $g(X) = X(X-3x_0)^2$ and $f(X) = (X - \mu_4 - x_0)(X - 3x_0)$, yielding that

$$\left(\frac{f}{g}\right)'(X) = -\frac{X^2 - 2(x_0+\mu_4)X + 3x_0(x_0+\mu_4)}{X^2(X-3x_0)^2} < 0$$

for $\mu_4 \in [0, -x_0]$ since the discriminant of the numerator is $4(x_0+\mu_4)(\mu_4 - 2x - 0) < 0$. This ensures that there is at most one small limit cycle to the right of x_0 and that the limit cycle is repelling.

The situation is now as follows. When μ_4 decreases from $-x_0$ the system has two limit cycles, a large attracting one (surrounding the cusp and the weak focus) and a small repelling one (surrounding the weak focus). The limit cycles must have disappeared before $\mu_4 = 0$. The only possibility how this can occur is through a cuspidal loop bifurcation occuring for some particular value of μ_4 in the interval $[0, -x_0]$, in which the small repelling limit cycle is transformed into a large also repelling one. The cuspidal loop is seen numerically for $\mu_4 \approx -0.844x_0$. The two large limit cycles then coallesce, numerically they have already disappeared for $\mu_4 = -0.84x_0$.

We now discuss the cuspidal loop bifurcation in more detail. Localizing at $X = x - x_0$ yields the system

$$\begin{aligned} \dot{X} &= y \\ \dot{y} &= -3x_0X^2 - X^3 + (\mu_4 - 2x_0)Xy - X^2y. \end{aligned} \tag{5.2}$$

Hence, we see that the Bogdanov-Takens point on the left is repelling (meaning that it leads to the creation of a repelling limit cycle in the unfolding) for $\mu_4 - 2x_0 > 0$, which is the case for any $\mu_4 > 0$.

Two generic types of cuspidal loops are possible. They were known for a long time by the experts on the subject, but a thorough study just appeared recently in [DRS96]. In both cases the passage through the loop implies the disappearance of a small limit cycle and the appearance of a large limit cycle:

1. both the cuspidal loop and the Bogdanov-Takens point are repelling. Then both the large and the small limit cycle are repelling;

2. the cuspidal loop is attracting and the Bogdanov-Takens point is repelling. Then both the large and the small limit cycle are attracting.

Whether the loop itself is attracting governs on which side of the bifurcation the small and the large limit cycle are, respectively. The first case requires an odd number of limit cycles around the cuspidal loop bifurcation, which is precisely the case. We could conclude that the first case occurs, if we knew that the situation is generic. A rigorous proof would require to show that the integral of the divergence along the cuspidal loop is positive. □

The above proposition shows that decreasing μ_4 leads to the birth of a small repelling limit cycle and to its transformation into a large one through the cuspidal loop. During the whole process everything is surrounded by a large attracting limit cycle. When μ_4 is decreased further the two limit cycles coallesce before $\mu_4 = 0$. This can only occur through a double limit cycle bifurcation.

Corollary 5.3 *There exists a positive value of μ_4 for which a double limit cycle coexists together with a Bogdanov-Takens bifurcation on the left (between* A *and* B*). This value is smaller than the value corresponding to the cuspidal loop.*

As a bonus of our calculations we get

Corollary 5.4 *The cusp of order three occurs at an equilibrium $x_1 > 0$ on the right at $\mu_4 = 2x_1$ (between* I *and* K*). There is no limit cycle at the moment of this bifurcation.*

Proof: The function $H(x,y) = y^2/2 + x_1x^3 + x^4/4$ is a Lyapunov function for (5.2) when $\mu_4 = 2x_1$, yielding that there are no limit cycles. □

Now the only missing piece in the transition is

Proposition 5.5
A simultaneous degenerate Hopf bifurcation on the right, with the saddle-node bifurcation on the left occurs for $\mu_4 = -\frac{5}{2}x_0$ (between H *and* I*).*

Proof:
Here again the saddle-node is located at $x = x_0 < 0$ and the weak focus at $x = -2x_0$. The divergence vanishes at $x = -2x_0$ if $\mu_3 = 2x_0\mu_4 + 4x_0^2$. We localize the system at the weak focus by $X = x + 2x_0$, yielding

$$\begin{aligned} \dot{X} &= y \\ \dot{y} &= -9x_0^2X + 6x_0X^2 - X^3 + Xy(\mu_4 + 4x_0) - X^2y. \end{aligned}$$

Letting $y = 3x_0Y$ and scaling time by $-3x_0$ gives

$$\begin{aligned} \dot{X} &= -Y \\ \dot{Y} &= X - \tfrac{2}{3x_0}X^2 - \tfrac{\mu_4+4x_0}{3x_0}XY + \tfrac{1}{9x_0^2}X^3 + \tfrac{1}{3x_0}X^2Y. \end{aligned}$$

The first Lyapunov quantity is then given by

$$V_1 = -\frac{2\mu_4 + 5x_0}{9x_0^2},$$

and the result follows □

The global bifurcations of (1.5) can also be studied by transforming the system to a near-Hamiltonian system. Here, again the local conic structure is expected to be found a posteriori from the bifurcation diagram.

6 Discussion of models

We mentioned earlier that the bifurcation diagram in Figure 2, or part of it, is found in all kinds of applications. Here we discuss two examples that illustrate different underlying mechanisms for this fact. We conjecture that if a model has a bifurcation diagram like in Figure 1 then it can either be directly translated into the form (1.2), or both equations have a common organizing center. We consider two types of organizing centers associated with the family (1.2): the codimension-four singularity corresponding to the limit $(\mu_1, \mu_2, \mu_3) \to (0, 0, 0)$, and the singular limit $(|\mu_1|, |\mu_2|, |\mu_3|) \to (\infty, \infty, \infty)$.

6.1 Bonhoeffer - van der Pol model

Consider the model

$$\begin{aligned} \dot{x} &= y - P(x) \\ \dot{y} &= \varepsilon(Q(x) - y), \end{aligned} \tag{6.1}$$

where

$$\begin{aligned} P(x) &= p_0 x^3 + p_1 x^2 + p_2 x + p_3, \\ Q(x) &= q_0 x^3 + q_1 x^2 + q_2 x + q_3, \end{aligned}$$

and $p_0 > q_0$, $p_0 > 0$ and $\varepsilon > 0$. We show below that this model is equivalent to either (1.5) or (1.2).

Proposition 6.1
System (6.1) can be transformed to the form (1.5). If additionally $q_1 p_0 = q_0 p_1$ *then (6.1) can be further reduced to the form (1.2) .*

Proof:
If we let $Y = y - P(x)$ then system (6.1) becomes

$$\begin{aligned} \dot{x} &= Y \\ \dot{Y} &= \varepsilon(Q(x) - P(x) - (1 + \frac{1}{\varepsilon}P'(x))Y). \end{aligned}$$

Scaling $(x, Y, t) \mapsto (x_1, y_1, T) = (\frac{1}{A}x, \frac{1}{B}Y, Ct)$, where $A = \sqrt{a}/b$, $B = a\sqrt{a}/b^2$, $C = a/b$, $a = \varepsilon(p_0 - q_0)$ and $b = 3p_0$, brings the coefficients of both cubic terms to -1. Finally, translating $x_1 \mapsto x_2 = x_1 - \bar{x}$, where

$\bar{x} = -(q_1 - p_1)/3A(q_0 - p_0)$, eliminates the x_2^2-term, and we obtain the form (1.5) with

$$\begin{aligned} \mu_1 &= \frac{\varepsilon}{BC}(Q(A\bar{x}) - P(A\bar{x})), \\ \mu_2 &= \frac{\varepsilon A}{BC}(Q'(A\bar{x}) - P'(A\bar{x})), \\ \mu_3 &= -\frac{\varepsilon}{C}(1 + \frac{1}{\varepsilon}P'(A\bar{x})), \text{ and} \\ \mu_4 &= -\frac{A}{C}P''(A\bar{x}). \end{aligned} \tag{6.2}$$

If $q_1 p_0 = q_0 p_1$ then $P''(A\bar{x}) = 2(p_1 - p_0(q_1 - p_1)/(q_0 - p_0)) = -2(q_1 p_0 - q_0 p_1)/(q_0 - p_0) = 0$, so that $\mu_4 = 0$. □

Obviously, the model (6.1) with $q_0 = q_1 = 0$ is of the form (1.2). Rychkov [Ry85] studies the model (6.1) for $q_0 = q_1 = q_3 = 0$. Bautin uses the same model for $q_0 = q_1 = p_3 = 0$ and $\varepsilon = 1$ to describe electrical circuits in [Ba75]. The bifurcation diagram of Bautin's model (see Fig. 1 in [Ba75]) coincides up to a rotation with the one in Figure 1(right). Note that Bautin uses the parameters $(\sigma, \lambda) = (q_3, -q_2)$, where $p_1 < 0$, $p_2 > 0$ and $p_1^2 - 3p_0 p_2 > 3p_0$. The last inequality means that μ_3 takes only positive values.

The following version of model (6.1)

$$\begin{aligned} \dot{x} &= y - x^3/3 + x \\ \dot{y} &= \varepsilon(\alpha - \beta x - y), \end{aligned} \tag{6.3}$$

where ε is small, called Bonhoeffer - van der Pol or Fitz-Hugh model [Gr87, VT94], frequently occurs in chemistry, biophysics and neural sciences. Its bifurcation diagram in the (α, β)-plane is like Figure 1 (right) as it corresponds to the slice $\mu_3 = const > 0$ of the bifurcation diagram of system (1.2). It is discussed particularly in [BDK80, Kh90, Kh97, Ry94, VT94]. The relation between the parameters of (6.3) and those of (1.2) is given by

$$\mu_1 = \frac{9\alpha\sqrt{3}}{\varepsilon\sqrt{\varepsilon}}, \quad \mu_2 = \frac{9(1-\beta)}{\varepsilon}, \quad \mu_3 = \frac{3(1-\varepsilon)}{\varepsilon}. \tag{6.4}$$

This shows that $\mu_2 > 0$ is equivalent to $\beta < 1$ and under this condition $(|\mu_1|, \mu_2, \mu_3) \to (\infty, \infty, \infty)$ when $\varepsilon \to 0$.

On the other hand, the limit $(\mu_1, \mu_2, \mu_3) \to (0, 0, 0)$ is equivalent to $(\varepsilon, \beta, \alpha) \to (1, 1, 0)$. So the bifurcation diagram in the (α, β)-plane of (6.3)

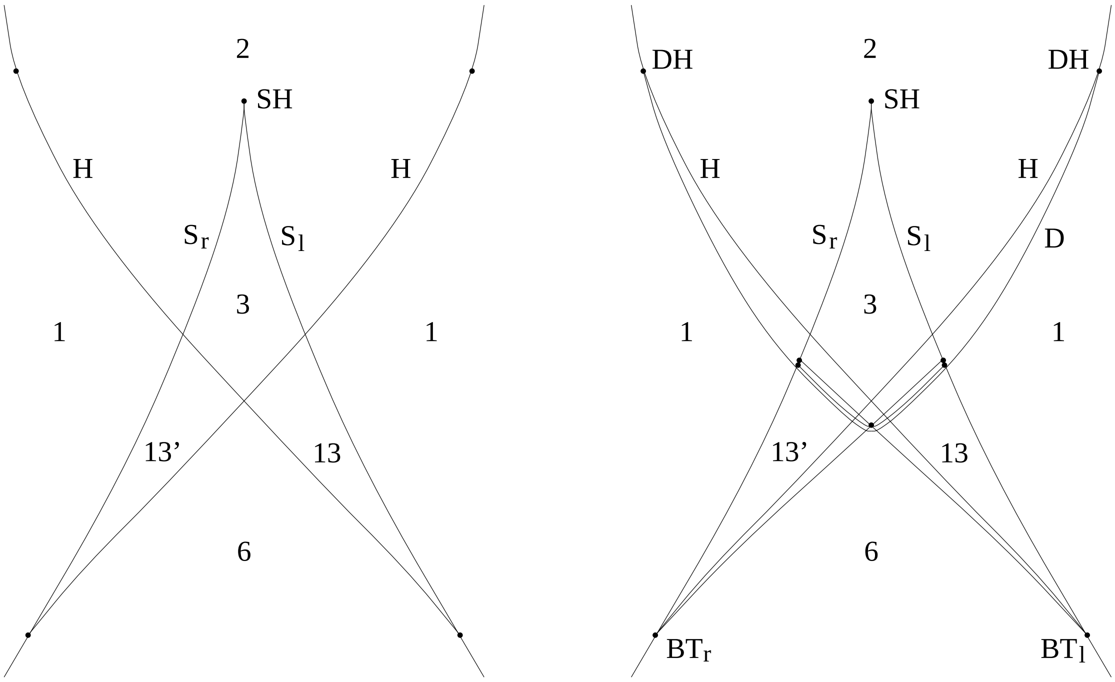

Figure 14: Sketch of the section $\mu_3 = const > 0$ in the singular limit (left), and close to the singular limit (right). The sketch reflects the fact that the global bifurcation curves converge to each other much faster (actually, exponentially fast) than the other curves.

for ε less but close to one correspond to the bifurcation diagram of (1.2) in the (μ_1, μ_2)-plane for small positive μ_3. In the (α, β)-plane of (6.3) the locus of Hopf bifurcations consists of the two lines $\alpha = \pm\frac{\sqrt{1-\varepsilon}}{3}(3\beta - \varepsilon - 2)$, the locus of saddle-node bifurcations consists of the two curves $3\alpha = \pm\frac{2}{3}(1-\beta)^{3/2}$, the cusp bifurcation point is $\alpha = 0, \beta = 1$, the Bogdanov-Takens points are $\alpha = \pm\frac{2}{3}(1-\varepsilon)^{3/2}$, $\beta = \varepsilon$, and the degenerate Hopf bifurcation points are $\alpha = \pm\frac{4}{3}(1-\varepsilon)^{3/2}$, $\beta = 2 - \varepsilon$.

As $\varepsilon \to 0$ the Hopf locus converges to $\alpha = \pm(\beta - \frac{2}{3})$, the "singular" Hopf locus defined by the condition that the y-nullcline crosses the x-nullcline (the slow manifold) at its critical point. The saddle-node locus does not change with ε, so that the local bifurcation diagram for $\varepsilon = 0$ is as shown in Figure 14 (left). It turns out that the global part of the bifurcation set also converges to the singular Hopf locus as $\varepsilon \to 0$. This means that the parameter regions 12,14,14',7,7',8,8',11,11' narrow and eventually shrink to line segments while regions 4,5,9,9',10,10' shrink to the point corresponding to simultaneous left and right Hopf bifurcations, as is illustrated in Figure 14 (right). Because of this remarkable simplification of the bifurcation diagram of (6.3) in the singular limit, it is natural to think of this limit as a different organizing center. In fact, this singular limit leads to the bifurcation diagram in Figure 1 in a wide range of applications that have two time scales. A more detailed discussion of this topic goes beyond the scope of the present paper. We refer to [Kh97, SL85] and discuss a related example below.

6.2 An ecological model

In this section we discuss the following ecological model from [BBIK93]

$$\begin{array}{rcl} \dot{x} & = & x(x-\ell)(1-x) - xy + \alpha \\ \dot{y} & = & -\gamma y(m - x + \delta y) \end{array} \tag{6.5}$$

for positive values of the parameters. This model is used to study various patterns of outbreaks of insect populations, in particular those associated with phase portraits 3, 6, 13 and 13'. The bifurcation diagram of this model (see Fig.2 in [BBIK93]) is equivalent to that shown in Figure 1(right). This similarity may be explained by two types of arguments.

First, we show that the full bifurcation diagram of system (6.5) contains parameters, so that there is a Z_2-equivariant nilpotent singularity. Consider the set of parameters satisfying

$$\begin{array}{rcl} l & = & x_0 \dfrac{3\delta^2\gamma x_0 + 1 + \delta\gamma - 2\gamma\delta^2}{\gamma\delta^2\,(2x_0 - 1)} \\ m & = & \dfrac{(-1+\delta\gamma)x_0}{\delta\gamma} \\ \alpha & = & -x_0^2 \dfrac{\delta^2\gamma x_0^2 + x_0(-2\delta^2\gamma - 1 + \delta\gamma) + \gamma\delta(\delta - 1)}{\gamma\delta^2\,(2x_0 - 1)}, \end{array} \tag{6.6}$$

for which there is a nilpotent singularity at $(x_0, y_0) = (x_0, -\frac{x_0}{\delta^2\gamma})$. Using (6.7) the system, localized at (x_0, y_0) by means of the change of variables

$(X, Y) = (x - x_0, y - y_0)$, becomes

$$\begin{aligned}
\dot{X} &= \frac{x_0}{\delta}X - x_0 Y - \frac{3\delta^2\gamma x_0^2 - 3\delta^2\gamma x_0 - x_0 - x_0\delta\gamma + \gamma\delta^2}{\gamma\delta^2(2x_0 - 1)}X^2 - XY - X^3 \\
\dot{Y} &= \frac{x_0}{\delta^2}X - \frac{x_0}{\delta}Y + \gamma XY - \delta\gamma Y^2. \qquad (6.7)
\end{aligned}$$

We now bring the linear part into Jordan normal form by the change of coordinates $(u, v) = (Y, \frac{x_0}{\delta^2}X - \frac{x_0}{\delta}Y)$, which finally leads to the system

$$\begin{aligned}
\dot{u} &= v + \frac{\gamma\delta^2}{x_0}uv \\
\dot{v} &= -\frac{6\delta^2\gamma x_0^2 - 6\delta^2\gamma x_0 - 2x_0 + 2\gamma\delta^2 - \gamma\delta + 2\gamma^2\delta^2 x_0 - \gamma^2\delta^2}{\gamma\delta(2x_0 - 1)}uv \\
&\quad -x_0\frac{3\delta^2\gamma x_0^2 - 3\delta^2\gamma x_0 - x_0 + x_0\delta\gamma + \gamma\delta^2 - \gamma\delta}{\gamma\delta^2(2x_0 - 1)}u^2 \\
&\quad -\frac{-x_0 + 3x_0^2\delta^2\gamma - x_0\delta\gamma - 3\delta^2\gamma x_0 + \delta^2\gamma}{\gamma x^0(2x_0 - 1)}v^2 \\
&\quad -\delta x_0 u^3 - 3\delta^2 u^2 v - \frac{3\delta^3}{x_0}uv^2 - \frac{\delta^4}{x_0^2}v^3. \qquad (6.8)
\end{aligned}$$

In general the coefficients of uv and u^2 in the second equation or (6.8) will be nonzero, which defines genuine Bogdanov-Takens bifurcations, but we can choose the parameters in such a way that both these coefficients are zero. By setting

$$\begin{aligned}
3\delta^2\gamma x_0^2 - 3\delta^2\gamma x_0 - x_0 + x_0\delta\gamma + \gamma\delta^2 - \gamma\delta &= 0 \\
6\delta^2\gamma x_0^2 - 6\delta^2\gamma x_0 - 2x_0 + 2\gamma\delta^2 - \gamma\delta + 2\gamma^2\delta^2 x_0 - \gamma^2\delta^2 &= 0
\end{aligned}$$

and using (6.7) we find the one-parameter family

$$\delta = \frac{1}{3x_0^2 - 3x_0 + 1}, \ \gamma = 3x_0^2 - 3x_0 + 1, \ l = 3x_0^2, \ \alpha = x_0^3, \ m = 0 \qquad (6.9)$$

for which the system has the form

$$\begin{aligned}
\dot{u} &= v + \frac{1}{(3x_0^2 - 3x_0 + 1)x_0}uv \\
\dot{v} &= -\frac{x_0}{3x_0^2 - 3x_0 + 1}u^3 - \frac{3}{(3x_0^2 - 3x_0 + 1)^2}u^2 v - \frac{3}{(3x_0^2 - 3x_0 + 1)^3 x_0}uv^2 \\
&\quad + \frac{2(x_0 - 1)}{(3x_0^2 - 3x_0 + 1)(2x_0 - 1)}v^2 - \frac{1}{(3x_0^2 - 3x_0 + 1)^4 x_0^2}v^3 \qquad (6.10)
\end{aligned}$$

Dividing both equations by $1 + \frac{1}{(3x_0^2 - 3x_0 + 1)x_0} u$ eliminates the uv-term in $\dot{u}$, while the coefficients of u^3 and $u^2 v$ remain unchanged in $\dot{v}$. After appropriate scaling we obtain the form (1.5) up to the higher order terms of order $O(u^4, v^2)$, which we expect do not alter the topological structure of the codimension-four unfolding conjectured in Figures 12 and 13. Based on this, we can now unfold family (6.10) with all positive parameters to obtain in system (6.5) the bifurcation diagram shown in Figure 1 (right).

A second argument is that the bifurcation diagram of (6.5) comes from singular perturbations; see [BBK97]. If we assume that γ is small then (6.5) becomes a fast-slow system. We let m and δ be the active parameters and find l and α such that the bifurcation diagram of system (6.5) for $\gamma = 0$ has qualitatively the structure as that of the Bonhoeffer - van der Pol equation in the limit $\varepsilon = 0$; see Figure 14(left). A possible choice is $l = 0.5$ and $\alpha = 0.05$; compare [BBK97]. For γ nonzero but sufficiently small we obtain the unfolded diagram of the same type as for Bonhoeffer - van der Pol equation shown in Figure 14 (right).

The singular perturbation approach in this context has the advantage over searching for a codimension-four singularity that it adds geometric insight based on the relative positions of the nullclines. As a consequence all relevant computations are simpler. Also, in this approach the desired phase portraits immediately emerge as normal scale objects (as opposed to small scale objects near a local singularity). This last observation seems to be especially relevant for the modeling of outbreak phenomena.

Acknowledgments

We thank A.R. Champneys and E. Doedel for their help with `HomCont` and `AUTO`, J. Guckenheimer for fruitful discussions and R.E. Kooij voor his comments on Section 5. A.K. was partly supported by a DOE grant and thanks CRM, University of Montréal for hospitatily and support during several visits. B.K. thanks the NSF Science and Technology Research Center for the Computation and Visualization of Geometric Structures (The Geometry Center, Minneapolis) for its hospitality and support under NSF/DMS89-20161, which made it possible to produce the 3D-viewer and the movie of the bifurcation set.

References

[AAIS94] V.I. Arnol'd, V.S. Afrajmovich, Yu.S. Il'yashenko and L.P. Shil'nikov, "I. Bifurcation Theory", in V. I. Arnol'd (Ed.), *Dynamical Systems V: Bifurcation Theory and Catastrophe Theory*, Encyclopedia of Mathematical Sciences **5**, Springer, Berlin, 1994.

[BGMWW92] A. Back, J. Guckenheimer, M.R. Myers, F.J. Wicklin and P.A. Worfolk, "DsTool: Computer assisted exploration of dynamical systems", *Notices Amer. Math. Soc.* **39** (1992), 303–309.

[Ba75] A.N. Bautin, "Qualitative investigation of a particular nonlinear system", *J. Appl. Math. and Mech.* **39** (1975), 633–641.

[BBIK93] A.D. Bazykin, F.S. Berezovskaya, A.S. Isaev and R.G. Khlebopros, "Parametric foundation of the stability principle of 'phytophage-entomophage' system dynamics", *Dokl. Russian Acad. Sci.* **333** (1993), 673-675.

[BBK97] A.D. Bazykin, F.S. Berezovskaya, A.I. Khibnik, "Bifurcation approach to forest insect dynamics" (in peparation).

[BKK85] A.D. Bazykin, Yu.A. Kuznetsov and A.I. Khibnik, "Bifurcation diagrams of planar dynamical systems", preprint, Research Computing Center, Pushchino, 1985 (in Russian).

[BK85] F.S. Berezovskaya and A.I. Khibnik, "Bifurcations in second order differential system with double zero eigenvalue and additional degeneracy", in *Methods of Qualitative Study of Differential Equations*, Gorkii, 128-138, 1985 (in Russian).

[BDK80] J. Boissonade and P. De Kepper, "Transition from bistability to limit cycle oscillations. Theoretical analysis and experimental evidence in an open chemical system", *J.Phys.Chem.* **84** (1980), 501-506.

[Ca81] J. Carr, *Applications of centre manifold theory*, Appl. Math. Sciences. **35**, Springer-Verlag 1981.

[CKS95] A.R. Champneys, Yu.A. Kuznetsov, B. Sandstede, "A numerical toolbox for homoclinic bifurcation analysis", *Appl. Nonlin. Math. Research Report* 1.95, University of Bristol 1995.

[Ch77] L.A. Cherkas, "Estimation of the number of limit cycles of autonomous systems", *J. Differential Equations* **13** (1977), 529–546.

[DG87] G. Dangelmayr and J. Guckenheimer, "On a four parameter family of planar vector fields", *Archive Rational Mechanics* **97** (1987), 321–352.

[DK86] E. Doedel and J. Kernévez, "Auto: Software for continuation and bifurcation problems in ordinary differential equations with applications", Technical Report, CalTech 1986.

[DFM93] E. Doedel, M. Friedman and A. Monteiro, "On locating homoclinic and heteroclinic orbits", Technical Report, Cornell Theory Center 1993.

[Du53] G.F. D. Duff, "Limit cycles and rotated vector fields", *Annals of Math* **67** (1953), 15-31.

[DL96] F. Dumortier and C. Li, "On the uniqueness of limit cycles surrouding one or more singularities in liénard equations", Nonlinearity **9** (1996), 1489-1500.

[DR90] F. Dumortier and C. Rousseau, "Cubic Liénard equations with linear damping", Nonlinearity **3** (4) (1990), 1015–1039.

[DRS87] F. Dumortier, R. Roussarie and J. Sotomayor, "Generic 3-parameter families of vector fields on the plane, unfolding a singularity with nilpotent linear part. The cusp case", *Erg. Th. & Dyn. Syst.* **7** (1987), 375-413.

[DRS91] F. Dumortier, R. Roussarie and J. Sotomayor, "Generic 3-parameters families of planar vector fields, unfoldings of saddle, focus and elliptic singularities with nilpotent linear parts", Springer Lecture Notes in Mathematics **1480** (1991), 1-164.

[DRS96] F. Dumortier, R. Roussarie and J. Sotomayor, "Bifurcations of cuspidal loops", preprint 93-103, Université de Bourgogne 1996.

[Gr87] J. Grasman, *Asymptotic methods for relaxation oscillations and applications*, Appl. Math. Sciences. **63**, Springer-Verlag 1987.

[HS74] M.W. Hirsch and S. Smale, *Differential Equations, Dynamical Systems, and Linear Algebra*, Academic Press, London 1974.

[KS75] N.P. Kaimachnikov and E.E. Sel'kov, "Hysteresis and multiplicity of dynamic states in an open two-substrate enzymatic reaction with substrate depression", *Biofizika* **20** (1975), 703-708.

[Kh90] A.I. Khibnik, "On generation of two-parameter bifurcation diagram by singular perturbation", *Nonlinear Oscillations in Mechanical Systems*, Gorkii (1990), 136-137 (in Russian).

[Kh97] A.I. Khibnik, "Global bifurcations associated with local bifurcations in fast-slow systems" (in preparation).

[KBY87] A.I. Khibnik, V.I. Bykov and G.S. Yablonskii, "23 phase portraits of the simplest catalytic oscillator", *Russian J. Phys. Chem.* **61** (1987), 722-723.

[Kh85] E.I. Khorosov, "Versal deformations of equivariant vector fields for the case of symmetries of orders 2 and 3", *Topics in modern mathematics*, Petrovskij Seminar 5 (1985), 207–243.

[Ku95] Yu.A. Kuznetsov, *Elements of Applied Bifurcation Theory*, Appl. Math. Sci. **112**, Springer-Verlag 1995.

[LRW90] C. Li, C. Rousseau and X. Wang, "A simple proof for the unicity of the limit cycle in the Bogdanov-Takens system" Bull. Can. Math. **33** (1990), 84-92.

[Ma94] S. Malo, "Rigorous computer verification of planar vector field structure", Ph.D.-thesis, Cornell University 1994.

[Pe75] L.M. Perko, "Rotated vector fields and the global behavior of limit cycles for a class of quadratic systems in the plane", *J. Differential Equations* **18** (1975), 63-86.

[Rou86] R. Roussarie, "On the number of limit cycles which appear by perturbation of separatrix loop of planar vector fields", *Bol. Soc. Bras. Mat.* **17** (1986), 67-101.

[Ry80] G.S. Rychkov, "Uniqueness of a limit cycle of the equation $(y - P_3(x))dy = P_1(x,y)dx$", *Differential Equations* **16** (1980), 269-272.

[Ry84] G.S. Rychkov, "The absence, for the equation $P_1(x,y)dx = (y - P_3(x))dy$, of limit cycles encircling three critical points", *Differential Equations* **20** (1984), 1357-1360.

[Ry85] G.S. Rychkov, "Maximum number of limit cycles of the equation $(y - P_3(x) = P_1(x, y)dx$ in the case of three critical points", *Differential Equations* **21** (1985), 668-672.

[Ry90] S.E. Reshetnikov and G.S. Rychkov, "Bifurcation values of parameters of the system $\dot{x} = y - \sum_{i=1}^{3} a_i x^i$, $\dot{y} = a_{10}x + a_{01}y$", *Differential Equations* **26** (1990), 579-582.

[Ry94] G. S. Rychkov, "Bifurcation values of parameters in the Fitz-Hugh equations", *Differential Equations* **30** (1994), 373-376.

[SL85] M. Sheintuch and D. Luss, "Dynamic features of two ordinary differential equations with widely separated time scales", *Chem. Eng. Sci.* **40** (1985), 1653-1664.

[VSA78] D.A. Vaganov, N.G. Samoilenko and V.G. Abramov, "Periodic regimes of continuous stirred tank reactors", *Chem. Eng. Sci.* **33** (1978), 1133-1140.

[VT94] E.V. Volokitin and S.A. Treskov "Parametric portrait of the Fitz-Hugh differential system", *Mathematical Modeling* **6** (1994), 65-78 (in Russian).

[WK92] X. Wang and R.E. Kooij, "Limit cycles in a cubic system with a cusp", *SIAM J. Math. Anal.* **23**(6) (1992), 1609-1622.

[Zh86] Z. Zhang, "Proof of the uniqueness theorem of limit cycles of generalized Liénard equations", *Applicable Analysis* **23** (1986), 63-76.